ADVANCING

MICROELECTRONICS

EVERYTHING IN ELECTRONICS BETWEEN THE CHIP AND THE SYSTEM!

MARCH/APRIL 2018
Vol. 45 No. 2

RF/Microwave High-Frequency High-Reliability

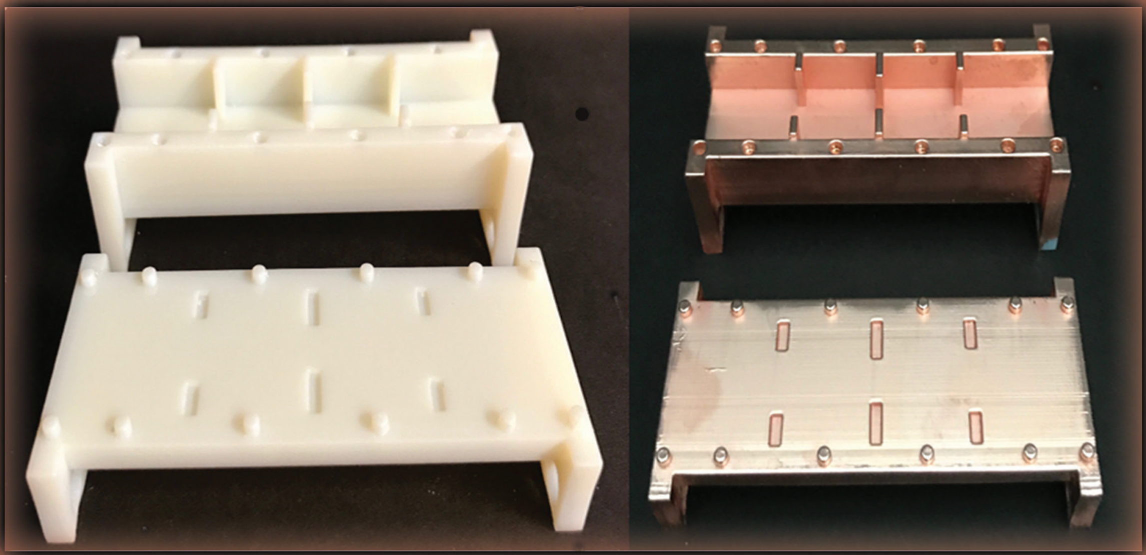

INSIDE THIS ISSUE

IMAPS 2017 Award Winners
Pages 22-23

PASADENA

iMAPS 2018

51st International Symposium on Microelectronics

October 8-11, 2018

Pasadena Convention Center



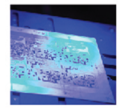

IMAPS 2018 - Pasadena

51st Symposium on Microelectronics

Conference:	Exhibition:
October 9-11, 2018	October 9-10, 2018

Professional Development Courses:
October 8, 2018

General Chair:
Mark Gerber
ASE US Inc.

General Chair-elect (2019):
Steffen Kroehnert
Amkor Technology (formerly Nanium)

Past General Chair (2017):
Dan Krueger
Honeywell FM&T

The 51st International Symposium on Microelectronics is being organized by the International Microelectronics Assembly and Packaging Society (IMAPS). The IMAPS 2018 Technical Committee seeks original papers that present progress on technologies throughout the entire microelectronics/packaging supply chain. The Symposium will feature 5 technical tracks, plus our Interactive Poster Session, that span the three days of sessions on:

TRACK 1: **SiP/SiM (System Solutions)**	TRACK 2: **Wafer Level/Panel Level (Advanced RDL)**	TRACK 3: **High Performance / High Reliability**	TRACK 4: **Flip Chip/2.5D/3D/ Optical (Advanced Package)**	TRACK 5: **Advanced Process and Materials (Enabling Technologies)**
PLANNED SESSIONS: • System Design & Integration • CPI and Modeling • Embedded/High Voltage • Optical / Automotive • Wearable / Test	PLANNED SESSIONS: • Wafer-level Fan Out • WLCSP • Advanced Fan Out • Panel-level Fan Out • MEMS & Sensors	PLANNED SESSIONS: • High Reliability in Defense and Aerospace • MM Wave / High-speed Packaging • RF / Wireless Components • High Reliability in Bio/Medical •High Reliability in Extreme Environments	PLANNED SESSIONS: • Large Body / Small Body FC • 2.5D Technologies • Optical • BUMP & Interconnect • 3D Technologies	PLANNED SESSIONS: • Substrate Technology • Polymer Materials & Processes • Novel Materials & Processes • Advanced Wirebond • Advanced Equipment & Additive Manufacturing
TRACK 6: **INTERACTIVE POSTER SESSION - *"Posters & Pizza Lunch"***				

PROGRAM AVAILABLE SOON: www.imaps2018.org

EXHIBITS FILLING FAST! *Phase II Application Period for Returning IMAPS 2017 Exhibitors Opened February 15th*
Phase III Open Application Period Begins at 12PM Eastern April 2nd

MARCH/APRIL
2018

ADVANCING MICROELECTRONICS

EVERYTHING IN ELECTRONICS BETWEEN THE CHIP AND THE SYSTEM!

Features

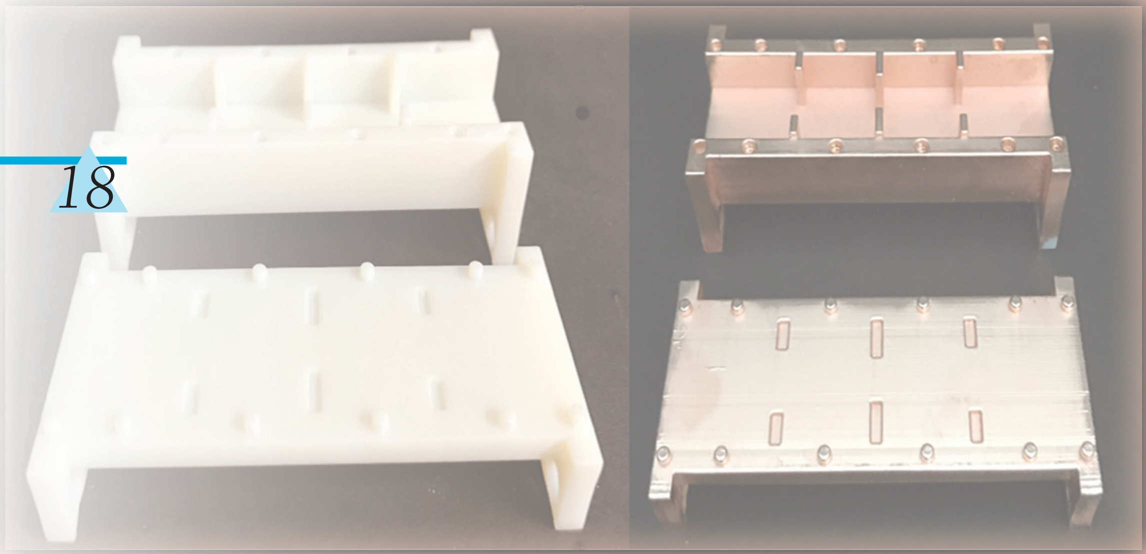

On the Cover:
Sections of the fabricated iris filter before and after metal coating.

CONTENTS

IMAPS 4-TIER PARTICIPATION

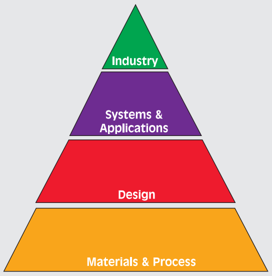

Industry

Systems & Applications

Design

Materials & Process

DEPARTMENTS

IMAPS 2017

UPDATES FROM IMAPS

MEMBER TOOLS

INSIDE BACK COVER

Correction

In the November/December issue we used an incorrect title for our Guest Editor.

Urmi Ray, Senior Director, Group Technology Strategy, STATS ChipPAC and IMAPS Vice President of Technology

IMAPS - International Microelectronics Assembly and Packaging Society
PO Box 110127
79 TW Alexander Dr.
4401 Building Suite 115
Research Triangle Park, NC 27709
USA
Tel: +1-919-293-5000
E-Fax: +1-919-287-2339

See us on IMAPS's Home Page:
www.imaps.org

COMING NEXT ISSUE

Heterogeneous Integration – System in Package (SiP)

UPCOMING EVENTS

International Conference and Exhibition on Device Packaging 2018
March 5-8, 2018 We-Ko-Pa Resort and Casino, Fountain Hills, Arizona

CICMT 2018 (Portugal)
April 18-20, 2018 University of Aveiro Aveiro, Portugal

IMAPS New England - 45th Symposium & Expo
May 1, 2018 Boxborough, MA

HiTEC 2018 - High Temperature Electronics
May 8-10, 2018 Albuquerque, New Mexico

Topical Workshop & Tabletop Exhibition on Wire Bonding
October 8, 2018 Pasadena, CA

IMAPS 2018 - Pasadena
October 8-11, 2018

Visit IMAPS.org to see all upcoming Advanced Technology Workshops and Conferences

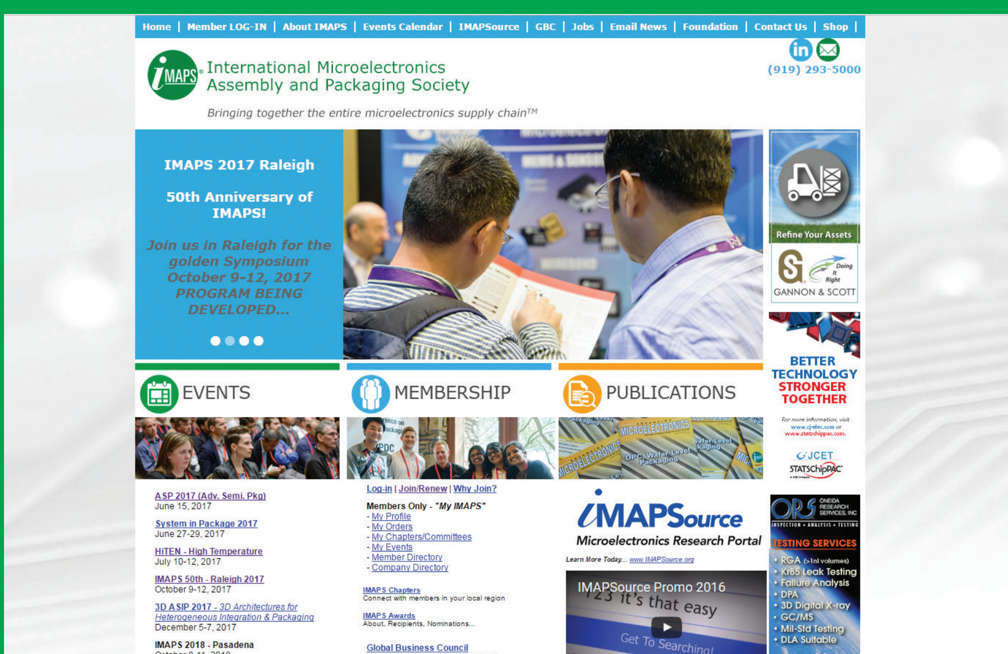

FROM THE GUEST EDITORS

Packaging for High Frequency and Reliability

Erica Folk
Process Integration Manager
Northrop Grumman

Ivan Ndip
Head of the Department of RF and Smart Sensor Systems
Fraunhofer IZM

Our society continues to expect more and more from systems and products that depend on the advancement of packaging, microelectronics and system-integration. These demands range from more capability in cell phones (e.g., for emerging 5G networks) to smarter cars to more capable satellites. Many of these advancements depend on operations at higher frequencies (especially in the millimeter-wave range) enabling higher performance, smaller packages, less weight and less power consumption. Additionally, some high performance applications require high reliability, particularly due to harsh environments.

With the growing emphasis and need for high frequency and high reliability products, IMAPS has established a working group to focus on this topic. IMAPS has always been looking for cutting edge technologies in microelectronics and packaging, and believes that this group will help streamline research efforts and publications in the field of high frequency and high reliability. Currently the working group is pulling together a structure for a focused track at the 51st International Symposium on Microelectronics in Pasadena, CA. Sessions in this track include "High Reliability in Defense and Aerospace," "mmWave/High-Speed Packaging," "RF/Wireless Components," "High Reliability in Biomedical" and "High Reliability in Extreme Environments."

In this issue, we have chosen three papers that exemplify what we are aiming to highlight and foster within the working group. These papers show the benefits and challenges working in this domain. These are rigorous as well as innovative approaches on how to execute these type of designs and applications considering both cost and performance.

The first paper featured in this issue explores the integration and miniaturization of a radar system for an un-manned vehicle. Working at a high frequency capable of producing high quality images on a drone has applications in remote sensing, weather prediction and military surveillance. Un-manned applications present a size restriction challenge that also lends itself to power and weight constraints. Operating at high frequencies allows for a smaller antenna paving the way for a Ka-band "card deck radar." While using LTCC and higher levels of integration, this paper demonstrates a 64 times size reduction, half power consumption and 10 times weight reduction from its predecessor.

Light weight, low cost and the ability to prototype are all features that are desired in the realm of high frequency. While some aspects of the physics of higher frequencies were exploited in the first paper to innately decrease the size and therefore the weight, waveguides which have historically been fabricated fully out of metal remain heavy for many applications. The authors of our second paper took an innovative approach and used 3D printing and metallized the plastic to produce a waveguide. This paper demonstrates a simple fabrication and assembly method and couples two well-known techniques – 3D printing and sputtering/electroplated metallization – to achieve and lighter and more cost effective waveguide.

In addition to high frequency, some high performance applications require high reliability. Automotive, space and drilling are some examples. Our third papers focuses on the relationship between time to failure and temperature as it applies to silver based thick film pads. This provides an economical, widely available solution. Results show good potential for this solution and provides a better understanding of the time to failure.

We hope that you enjoy reading these papers and learning about how they are pushing the limits in the domain for high frequency and high reliability. As we continue to develop the working group and determine how to best offer benefit to IMAPS members and greater packaging and microelectronics community in this field, we would appreciate your input. If you have cutting edge research in the field of high frequency and high reliability, we encourage you to submit an abstract to upcoming IMAPS symposia and conferences to make this track a strong one for years to come! We also encourage you to join the working group on high frequency and high reliability.

IMAPS JOBS MarketPlace

Your IMAPS membership provides you with the on-line JOBS MarketPlace. This is a proactive, valuable, complimentary member service for both job seekers and prospective employers. Take advantage of it to find open positions or fulfill staffing needs.

IMAPS members can post unlimited job openings at no cost. Hiring managers can search for and view resumes of industry participants at no cost by using convenient sort criteria.

Member job seekers can post resumes and/or search for current openings at no cost. Job seekers can make their search even easier by setting up a job alert so compatible openings (by industry, location, and job function criteria) will be e-mailed as they are posted.

Find out more information at http://jobs.imaps.org/home

Integration and Miniaturization of a Ka-band Stepped Frequency Radar for Un-manned Aerial Vehicle Applications

Jay W. McDaniel, Mark B. Yeary and Hjalti H. Sigmarsson
University of Oklahoma, School of Electrical and Computer Engineering
Advanced Radar Research Center, 3190 Monitor Ave., Norman, OK 73071
Ph: 785-817-6599, Email: jmcdaniel@ou.edu

J. Ambrose Wolf, Sean Garrison, Kyle Byers and Matthew Clewell
Department of Energy's Kansas City National Security Campus,
14510 Botts Rd., Kansas City, MO 64147, Ph: 816-488-2000, Email: awolf@nsc.com

Abstract

In this paper, we present a highly integrated and miniaturized Ka-band stepped frequency radar that can be used for un-manned aerial vehicle applications. The microwave portion of the radar is integrated onto a low temperature co-fired ceramic multi-chip module, utilizing a triple-print gold thick-film metallization, allowing for wire-bonding and solder capabilities. In addition to miniaturization, a metal seal frame was designed to surround the individual microwave circuits providing isolation barriers to reduce electromagnetic coupling within the system and disturbances from outside interferers. The radar implementation is based on a previous Ka-band radar system designed at the University of Oklahoma using connectorized commercial-off-the-shelf components. This new design results in a 64 times size reduction in foot-print area, half the power consumption, and greater than a 10 times weight reduction compared to the previous implementation. To ensure desired system performance is maintained, both radars were subjected to a direct loop-back test and the intermediate frequency output spectrums, prior to base-band down-conversion, are recorded and compared. Both outputs contain a spectrally pure tone at 12.8 GHz near the expected power indicating that the new radar performs as intended and is comparable to its predecessor. The packaging techniques presented show extreme promise for system integration and miniaturization of future radar and communication systems following the trend to reduce size, weight, and power.

Key words

low temperature co-fired ceramic, stepped frequency radar, system integration, un-manned aerial vehicle

I. Introduction

Modern day radar and communication systems are continuously being challenged to reduce their size, weight, and power (SWaP) in order to operate on smaller platforms such as un-manned aerial vehicles (UAVs) [1], due to direct applications in remote sensing of environments [2], severe weather [3], and military surveillance. One approach to reduce SWaP is to operate at higher frequencies, where the physical size of the microwave component decreases due to reductions in electrical length [4]. This is most noticeable in antenna length and aperture size [5], but applies to other RF and microwave components such as filters and power dividers.

Another approach is to move away from connectorized commercial-off-the-shelf (COTS) components and integrate subsystems or the entire system onto printed circuit boards (PCB) using surface mount (SMT) components [6]-[7]. A more advanced approach, which allows for even more compact designs, is achieved with multi-chip modules (MCM). This is accomplished by placing several bare die, usually performing multiple RF tasks on a single chip, which are connected together by wire-bonding the die to an underlying substrate with microwave transmission lines. This technology has been demonstrated on low temperature co-fired ceramic (LTCC) [8]-[9].

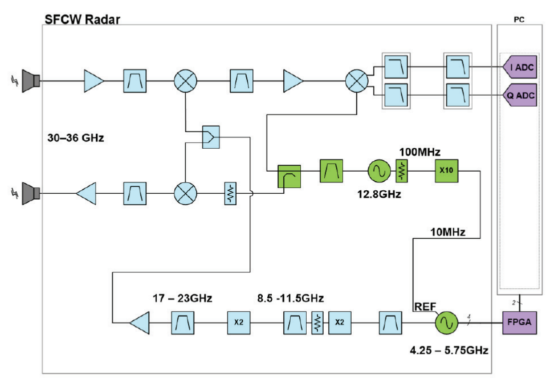

Figure 1: A typical Ka-band SFCW radar block diagram.

When combining the two approaches mentioned above for highly integrated radar and communication systems, requiring high transmitter (Tx) and receiver (Rx) isolation, the circuit design becomes more daunting due to the increased electromagnetic coupling within the system. Therefore, additional packaging techniques described throughout [10] must be further explored.

This paper presents a new highly integrated Ka-band stepped frequency radar implemented on a DuPont 9K7

Honeywell Federal Manufacturing & Technologies is operated for the United States Department of Energy under Contract Number - DE-NA-0002839.

LTCC [11] stack-up utilizing the MCM concept. In order to verify the system operation and performance, both the connectorized and integrated systems were subjected to a direct loop-back measurement and the results are compared.

II. Ka-Band Stepped Frequency Radar Design

A. Connectorized Radar

The Ka-band radar is a stepped frequency continuous wave (SFCW) system that transmits a 30 - 36 GHz waveform in increments of 20 MHz. An example of a typical SFCW radar block diagram can be found in Figure 1 [12]. The blue, green, and purple components make up the RF front-end, local oscillator (LO) section, and digital back-end, respectively. The original SFCW radar, designed at the University of Oklahoma, was constructed using coaxial microwave components and evaluation boards.

The LO section of the SFCW radar consists of two LO sources. LO1 is tunable from 4.25 - 5.75 GHz in 5 MHz steps, and is frequency quadrupled to produce a 17 - 23 GHz chirp in increments of 20 MHz. This signal is then split and used by both the Tx and Rx mixer to up-convert and down-convert, respectively. This LO is implemented using an EM Research SLS-5750 synthesizer. LO2 is a 12.8 GHz oscillator used for up-conversion in the Tx and as the RX in-phase and quadrature (I/Q) demodulator input to create the baseband I/Q data. The I/Q data is then used in signal processing to extract vital information of the target.

The transmit section outputs a continuous wave (CW) signal in frequency (F_{TX}):

$$F_{TX} = 4F_{synth} + 12.8\ GHz \qquad (1)$$

where F_{synth} is the output of the EM Research synthesizer. The resulting 30 - 36 GHz waveform is then filtered, amplified, and radiated through a rectangular horn antenna.

The receiver section captures the 30 - 36 GHz signal through a duplicate rectangular horn antenna and is immediately amplified by a low noise amplifier (LNA) to set the sensitivity of the radar. The signal is filtered and down-converted using LO1 to 12.8 GHz, where it is again amplified and down-converted using LO2 to produce the desired baseband I/Q data. The baseband data is low-pass filtered twice with the first filter providing high frequency attenuation and the second filter providing a quick roll-off to set the IF bandwidth. The final signal is then digitized by a 1 Msps National Instruments analog to digital converter.

B. Integrated Ka-band Radar

With the desire to implement the previous system on a UAV, it is essential to reduce the footprint of the radar to fit within the restricted space of a given platform. An initial investigation to minimize the RF front-end of the connectorized radar was proposed and is the primary focus throughout this paper. By integrating the entire front-end onto a single board, the system can be miniaturized into a nice compact design, but the performance can be improved by reducing the number of internal reflections from each connector. The packaged die were replaced with wire-bonded bare die. Additionally, the RF filters and Wilkinson power divider were integrated into the LTCC substrate using micro-strip technology. In addition, a drop-in version of the mixer was acquired to allow for mixer integration. The entire RF front-end was implemented on a LTCC stack-up, which will be discussed in the next section along with the integrated filters and power divider. Figure 2 shows a block diagram of the new integrated radar, referred to as the "card deck" radar throughout the rest of the text.

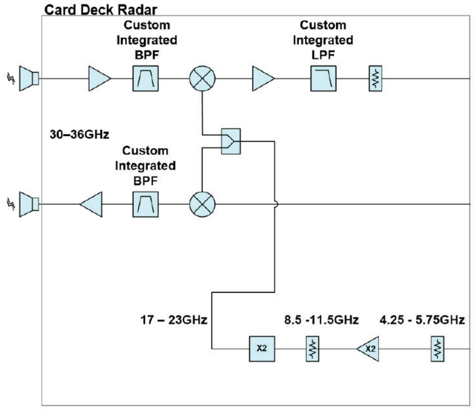

Figure 2: Block diagram of the Ka-band SFCW card deck radar.

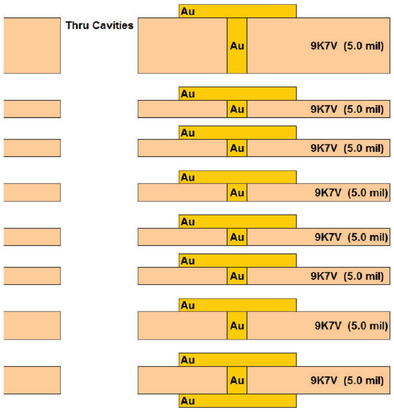

Figure 3: Card deck radar 8 layer LTCC stack-up.

III. LTCC Stack-up and Design

The card deck radar was designed on an eight substrate layer LTCC stack-up shown in Figure 3. The individual layers are 5-mil-thick 9K7V LTCC (ε_r = 7.1 and $tan\delta$ = 0.0010) in 5-inch panel forms. The individual panels are 4.27-mil-thick after firing resulting in a total 8-layer stack-up thickness of 34.16 mil. A triple print gold paste thick film process was used for all metallization layers.

The overall thickness needed to be around 30 mil in order to incorporate the Marki Microwave drop-in mixers [13] because the carrier board that the mixer die is attached to has a total thickness of 30 mil. This placed the top of both boards on the same horizontal plane allowing the wire-bond lengths to be minimized for maximum frequency operation. Per the recommended notes, the mixer was mounted to the LTCC substrate with silver epoxy to ensure a constant RF ground and eliminate RF interference with the mounting screws.

In addition, the eight layers were required in order to internally integrate the Ka-band band-pass filter. The designed filter is a substrate integrated waveguide evanescent combline filter [14] with a 30 - 36 GHz passband. By fully-integrating the filter within the LTCC stack-up and eliminating the bulky connectors, a size reduction of

continued on page 8

continued from page 7

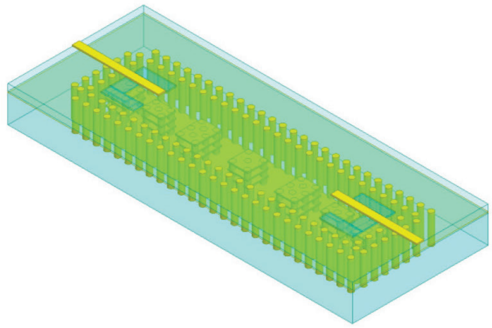

Figure 4: HFSS model of Ka-band evanescent band-pass filter.

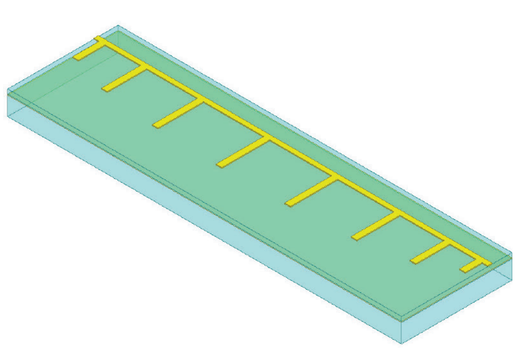

Figure 5: HFSS model of Ku-band low-pass micro-strip filter.

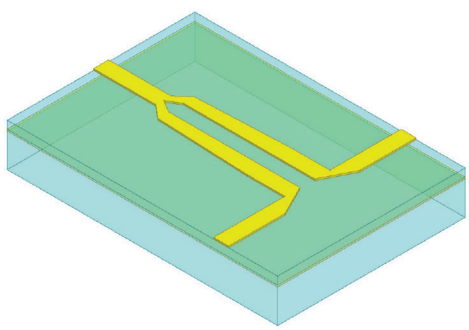

Figure 6: HFSS model of Ku-band Wilkinson power divider.

30x was achieved. An image of the Ansys HFSS model is shown in Figure 4. A Ku-band low-pass filter and Wilkinson power divider were also integrated onto the LTCC MCM. The low-pass filter was implemented as a micro-strip stub filter and designed to have a 1 dB cut-off frequency at 13 GHz [15]. A stopband attenuation of 30 dB at 17 GHz and 40 dB at 30 GHz was designed in order to attenuate the LO and RF leakage signals in the mixer. An image of the HFSS model for the low-pass filter is shown in Figure 5. Last, a 2-way Wilkinson power divider [16] was designed and integrated onto the board to split the LO signal to the two conversion mixers. The integrated Wilkinson power divider had less than 1 dB of insertion loss beyond 3 dB, due to 2-way power splitting, and provided greater than a 35 times size reduction compared to commercially available coaxial modules. Although a

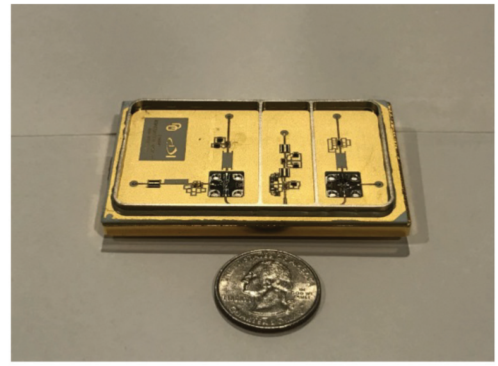

Figure 7: Fabricated Ka-band SFCW card deck radar.

smaller surface mount option could have been used, with similar size foot-print as the integrated power divider, they traditionally have additional loss due to the packaging. The HFSS model is provided in Figure 6.

The LTCC MCM is attached to a back-plate which provides adequate heat dissipation and structural support. All of the signals are brought on and off the board through GPPO connectors soldered into the back-plate. The center pin of the GPPO extends through the stack-up with through vias appropriately spaced in concentric circles around the pin in order to replicate a 50 ohm characteristic impedance coaxial transmission [17]. A lead-frame is soldered to the LTCC to complete the electrical connection between the center pin and microwave transmission lines. A conductor backed coplanar waveguide (CPWG) transmission line was used with a 5.2-mil-wide center trace and 5-mil-gap width. The CPWG trace was via-stitched with 5-mil-diameter vias in order to increase the CPWG bandwidth and ensure proper match to the highest frequency of interest.

Due to the high frequency operation of the SFCW radar, as well as the highly integrated MCM design, it was necessary to isolate the individual subsystems. The isolation can greatly be improved by surrounding the individual subsystems with a metal wall, and placing a metal lid on top of the walls. Small grooves were made in the lid for alignment with the seal-frame walls allowing the lid to lay flush across the circuit board. This ensured that any radiated fields that could couple to the nearby sensitive circuits would be terminated by the grounded structure. A photo of the fabricated card deck radar is shown in Figure 7.

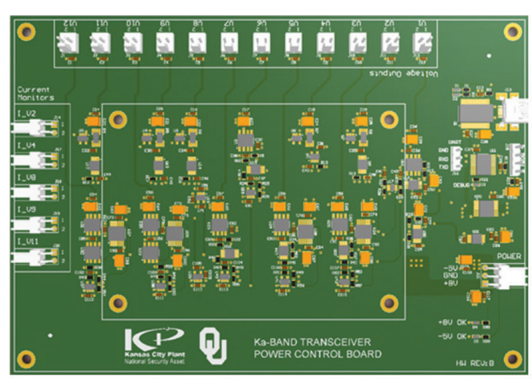

Figure 8: Image of power distribution board.

IV. Power Distribution Board Design

The power distribution board, shown in Figure 8, is responsible for providing the 12 voltage outputs to the card deck radar with only a +8V and -5V input. Seven of the voltages are fixed in hardware with five of the voltages being variable for gate voltage tuning using a 256-tap digital potentiometer (DPOT). Each of the outputs can be individually enabled or disabled via the enable (EN) line of the output's voltage regulator.

The states of the outputs are programmed via a USB-UART bridge on the board. An embedded microcontroller processes the message received from the bridge and sets the output of the power board accordingly. The board can be controlled by the user via a LabVIEW interface. Because the power board will be used to bias amplifiers and frequency doublers with specified power-on and power-off sequences, an additional feature was included to choose the power sequence along with associated time delays.

Once a suitable configuration is found, it can be stored to the on-board flash memory of the microcontroller by clicking the program button on the LabVIEW interface. If a configuration is stored to the flash, it will automatically be recalled the next time the power board is turned on without the need for the LabVIEW program.

V. SWaP Reduction

The final size of the card deck radar is 2 by 3 inches for a total area footprint of 6 in^2. The area of the original connectorized radar was 25 by 15.5 inches for a total area footprint of 387.5 in^2. Therefore, a 64 times area reduction has been accomplished. Also, the power consumption of the connectorized radar was 13.54 Watts, with the majority of that coming from the +12V biasing of the IF amplifier. The card deck radar cut the power consumption in half by only requiring 6.74 Watts. Finally, a significant weight reduction was also achieved. The total weight of the connectorized radar came in at 10.2 pounds, while the card deck radar weighed less than 1 pound.

VI. Loop-back Measurement and Results

A. Connectorized Radar

To develop a baseline reference, the connectorized radar was placed in a direct loop-back test setup. This works by connecting the output of the transmitter directly to the input of the receiver and measuring the IF output spectrum with a spectrum analyzer (SA) to verify output frequency and power level. All the voltages were supplied with two BK Precisions 9130 triple output DC power supplies. To simplify the test, a single +10 dBm 5 GHz tone from an Agilent Technologies E8257D analog signal generator was inserted into the LO1 frequency multiplier (FM) chain. This tone was then quadrupled to 20 GHz and fed into the Tx for up-conversion. The 12.8 GHz LO2, generated from LO1, was used to up-convert the 20 GHz LO1 to 32.8 GHz. The output of the Tx was connected to the Rx through a 2.92 mm cable and 20 dB attenuator. The 32.8 GHz signal was then down-converted to 12.8 GHz and amplified, where it was tapped off and sent into an Agilent Technologies E4448A SA to determine the spectral purity, ideal spectrum containing no harmonics, and power level at the IF output. The benchtop test setup is shown in Figure 9.

Figure 9: Test setup of the Ka-band SFCW connectorized radar.

Since the IF output of the receiver was tapped off prior to baseband down-conversion, a 12.8 GHz tone should appear on the SA. Calculations indicate that the power of this tone should be -14.5 dBm. As seen in Figure 10, the output of the radar is pure with a single 12.8 GHz tone at -14.89 dBm. The minor difference in calculated vs. measured power levels was most likely due to internal reflections within the system, due to mismatch between the higher frequency components.

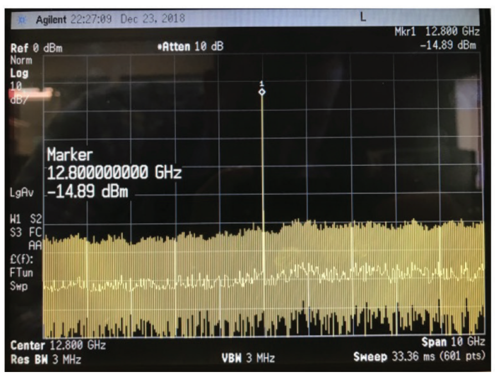

Figure 10: Ka-band SFCW connectorized radar output spectrum.

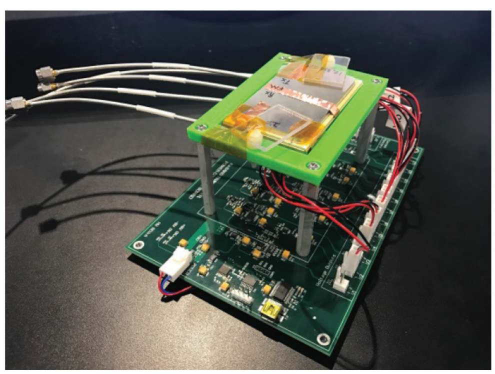

Figure 11: Fully-built Ka-band SFCW card deck radar.

B. Integrated Ka-band Radar

The fully built card deck radar, shown in Figure 11, was subjected to the same direct loop-back measurement with the only difference being the voltages were supplied with the custom designed power distribution board. The

continued on page 10

continued from page 9

bench-top test setup for this measurement is shown in Figure 12. Again, the output spectrum should be a spectrally pure 12.8 GHz tone with a power of -14.5 dBm. The output spectrum, shown in Figure 13, clearly displays a 12.8 GHz tone at -14.62 dBm. Comparing this result to the connectorized radar, it is evident that the card deck radar performs on par with the previous system and verifies our proof-of-concept MCM radar. There is a slight improvement in output power, which is most likely due to elimination of the SMA connectors and associated internal reflections.

Figure 12: Test setup of the Ka-band SFCW card deck radar.

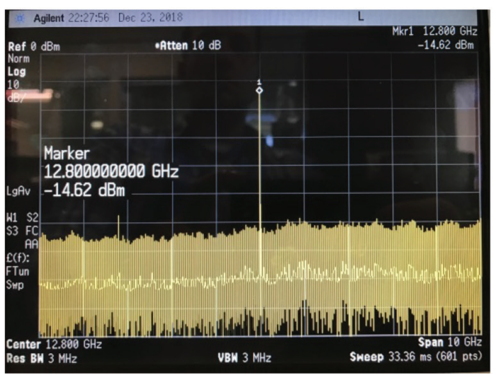

Figure 13: Ka-band SFCW card deck radar output spectrum.

VII. Conclusion

A highly integrated and miniaturized Ka-band SFCW radar on LTCC was designed providing a 64 times size, half power consumption, and 10 times size reduction. The seal-frame provides exceptional isolation and eliminates the electromagnetic coupling fields within the MCM package. Both the connectorized and integrated radar were subjected to a direct loop-back measurement and output spectrum results were analyzed and compared. Both outputs were spectrally pure containing a 12.8 GHz tone with power levels almost identical to the calculated value, confirming the MCM design. This technology shows significant size and weight improvements, while maintaining desired system functionality. The packaging techniques discussed will be crucial to the design and integration of high fidelity radar systems resulting in miniaturized packages that are capable of being flown on UAV platforms.

VIII. Acknowledgment

The authors would like to thank Matt Kempin for design and integration of the Ka-band evanescent combline filter, Kansas City National Security Campus for fabrication of the LTCC MCM, and Sandia National Labs, specifically Ken Peterson, for die attach and wire-bonding.

This work is funded by the Department of Energy's Kansas City National Security Campus (KCNSC), operated and managed by Honeywell Federal Manufacturing & Technologies, LLC (Contract Number: DE-NA0002839).

References

[1] K.H. Jones and J. Gross, "Reducing size, weight, and power (SWaP) of perception systems in small autonomous aerial systems," in *14th AIAA Aviation Tech., Integration, and Operations Conference,* 2014.
[2] C. Leuschen et al., "UAS-based radar sounding of the polar ice sheets," in *IEEE Geosci. and Remote Sens. Mag.,* vol. 2, no. 1, pp. 8-17, March 2014.
[3] National Research Council, *Weather Radar Technology Beyond NEXRAD*, Washington, DC: National Academy Press, 2002. Print.
[4] D.M. Pozar, *Microwave Engineering.* Hoboken, NJ: J. Wiley, 2012. Print.
[5] C.A. Blanis, *Antenna Theory.* Hoboken, NJ: J. Wiley, 2005. Print.
[6] J.W. McDaniel, J.B. Yan and S. Gogineni, "Design, integration, and miniaturization of a multichannel ultra-wideband snow radar receiver for airborne remote sensing," in *Microwave Journal*, 2016.
[7] E.C. Zaugg, D.L. Hudson and D.G. Long, "The BYU μSAR: a small student-built SAR for UAV operation," in *Proc. Int. Geosci. Rem. Sen. Symp.*, Denver, Colorado, pp. 411-414, Aug. 2006.
[8] R. Kulke, C. Gunner, P. Uhlig and M. Rittweger, "LTCC multi-chip modules for Ka-band multi-media satellite technology," in *German Microw. Conf.*, Germany, 2008, pp. 1-4.
[9] L. Zhong-yun, Z. Geng-hua, C. Peng and Y. Jian-yu, "Design and implementation of a LTCC-based receiver front-end module," in *2010 Int. Conf. on Microw. and Millimeter Wave Techn.,* Chengdu, 2010, pp. 1053-1056.
[10] C.R. Paul, *Electromagnetic Compatibility.* Hoboken, NJ: J. Wiley, 2006. Print.
[11] DuPont, "DuPont GreenTape low temperature co-fired ceramic system," DuPont 9K7 datasheet, Sept. 2009.
[12] J. Park and C. Nguyen, "A Ka-band stepped-frequency radar sensor for surface and subsurface sensing," in *2007 IEEE Antennas and Propag. Soc. Int. Symp.*, Honolulu, HI, 2007, pp. 4921-4924.
[13] Marki Microwave, "Double-balance mixers, M9-0942," Marki Microwave datasheet, Nov. 2013.
[14] S. Nassar. *An Investigation of the Equivalence Between Combline and Evanescent-mode Waveguide Filters & of Aspects Related to Reduction of Manufacturing Costs of Combline Filters.* Thesis. Stellenbosch University, 2011.
[15] G. Matthaei, L. Young and E.M. Jones, *Microwave Filters, Impedance-Matching Networks, and Coupling Structures.* NY: McGraw-Hill Book Co., 1964. Print.
[16] S.B. Cohn, "A class of broadband three-port TEM-mode hybrids," in *IEEE Trans. Microw. Theory Techn.*, vol. 16, no. 2, pp. 110-116, February 1968.
[17] R.E. Amaya, M. Li, K. Hettak and C.J. Verver, "A broadband 3D vertical microstrip to stripline transition in LTCC using a qusi-coaxial structure for millimeter-wave SOP applications," in *40th European Microw. Conf.*, Paris, 2010, pp. 109-112.

3D Printed Metallized Plastic Waveguides for Microwave Components

Mohd Ifwat Mohd Ghazali, Kyoung Youl Park and Premjeet Chahal
Department of Electrical and Computer Engineering
Michigan State University, East Lansing, Michigan
Email: chahal@msu.edu

Abstract

This paper investigates the design and fabrication of 3D printed waveguides and their application for the design of microwave passive components. This includes a simple waveguide structure, a bandpass filter, waveguide power splitter, a leaky wave antenna and a slot antenna array. A Lego-like approach is used to assemble different 3D printed sub-sections after metal coating. Details of modeling, fabrication and measurement results are presented, and simulation and measured results match closely.

Keywords
waveguide, 3D printing, additive manufacturing, Lego-like assembly, electroplating, leaky wave antenna, slot-array antenna, waveguide iris filter

I. Introduction

Lightweight and low-cost microwave components are required for spaceborne and satellite communications, automotive and hand-held systems [1-2]. Waveguides are broadly used for a variety of low-loss components such as filters, resonators, attenuators, and antennas. Hollow metallic waveguides are preferred over other waveguides due to their low-loss, high power handling capability, and improved isolation between neighboring structures [3]. In spite of these advantages, metallic waveguides are expensive to manufacture, and also due to the use of solid metal these waveguides are heavy. Metal waveguide structures are typically fabricated using techniques such as metal plate soldering, electroforming, dip-brazing and electronic discharge machining [4-5].

Additive manufacturing (AM) or 3D (3-dimensional) printing holds significant potential to lower the cost and weight while adding the ability to easily fabricate complex geometries [6-8]. Recently, many microwave, millimeter-wave and terahertz (THz) components with complex structure designs have been successfully demonstrated using 3D printing. Metal 3D printing by laser sintering is the most common technique to additively manufacture metal parts layer by layer. Most of the direct metal 3D printing techniques have a high surface roughness which can degrade the performance, especially at high frequencies [9]. Alternatively, 3D plastic printing and subsequent metallization have been utilized to achieve a smooth surface and lighter weight. Recently, many common RF components such as patch antennas, Vivaldi antennas have been successfully demonstrated from metal coated 3D printed plastics [10-11]. 3D printed plastic followed by electroless- or electro-plating has also been utilized in the manufacturing of waveguide structures [12-13].

This paper presents the fabrication of metal coated 3D printed plastic waveguides and its utility in the design of X-band passive components such as filters, antennas, and antenna arrays. To achieve good metal coating, each of the passive components is bisected and printed in separate pieces, metallized and then assembled using a Lego-like technique. Furthermore, it allows for the fabrication of multi-level waveguide components. All of the components here are printed using a professional-grade commercially available 3D printer (Objet Connex350) utilizing a photopolymer resin called "VeroWhitePlus." Although the dielectric properties are not critical, as the parts will be coated with metal films, it has a dielectric constant (ε_r) of ~2.8 and a loss tangent ($\tan\delta$) of ~0.04 measured over a frequency range of 0.1 - 1 0.8 THz [14] and has similar properties at lower frequencies. Both clear and white colored resins were utilized here in the fabrication of waveguides. All the structures were blanked metallized, and all the design and simulations were validated using a commercially available FEM simulation tool, ANSYS HFSS (High Frequency Structural Simulator).

II. Fabrication

The waveguide structures are printed in two separate layers as shown in Figure 1. Lego-like support pillars and holes are printed to allow the two layers to snap together with each other for proper alignment. After print, the structures are first cleaned using iso-propyl alcohol (IPA) placed in an ultrasonic bath, and they are subsequently cured under UV light. Blanket metallization of 3D printed structures is carried out using a two-step process. First, a seed layer of Titanium/Copper (Ti/Cu: 100nm/500nm) is blanket sputter deposited on all sides. The Ti layer acts as the adhesive layer between Cu and the plastic. Second, a thick layer (~5 µm) of Cu is electroplated. The structures are then assembled together as depicted in Figure 1(c). The measured surface roughness of the inner walls is approximately ~5 mm. Figure 1(d) shows an example 3D printed waveguide structure after metal coating. A thin layer of highly conductive silver paste was used to permanently join the pieces together.

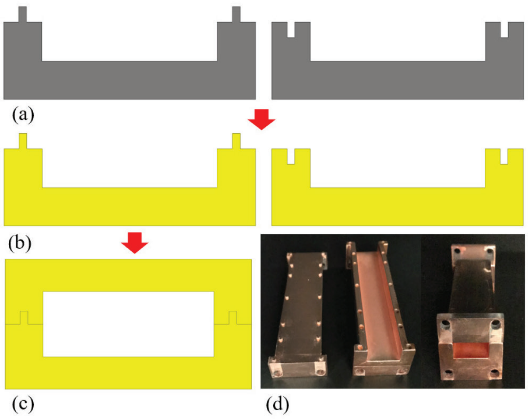

Figure 1. (a) 3D printed plastic parts, (b) parts are blanket metallized, (c) the parts are snapped together, (d) shown is an example waveguide after metallization.

III. Simulation and Measurement

A. X- and K-band Rectangular Waveguides

Rectangular waveguides are commonly used for low-loss high power handling applications. The cut-off frequency depends on the dimensions of the inner hollow region. For the X-band (8 – 12 GHz) design, the dimensions used are: width (a) = 22.86 mm, height (b) = 10.16 mm and length = 100 mm as shown in Figure 2. For the K-band (18 – 27 GHz) design, the dimensions used are: width (a) = 10.67 mm, height (b) = 4.32 mm and length = 50 mm. The printed waveguides, before metallization, are shown in Figure 3. The X-band waveguide after metallization is shown in Figure 1(d). For the measurements, these 3D printed straight sections were attached to broadband waveguide adaptors at each end. Using a vector network analyzer, VNA (N5227A), the S-parameters of these waveguides were measured over 5 – 13 GHz frequency range.

Figure 4 shows the simulated and measured S-parameters for the X-band waveguide. Overall, the simulation and measurement results match closely. The discrepancy can be attributed to surface roughness, fabrication tolerances of the printer (~ ± 25mm) and the potential air gap between the two pieces when snapped together due to small warpage along the length. Furthermore, there is a slight misalignment between the coupler and the waveguide which leads to impedance mismatch. Figure 5 shows the measured and simulated S-parameters of the K-band waveguide. Here also the simulation and measured results match closely. The discrepancy here also is largely due to surface roughness and misalignment between the coupler and the waveguide. However, in both waveguide designs, the loss is less than 0.1dB/mm which shows significant promise of these printed components.

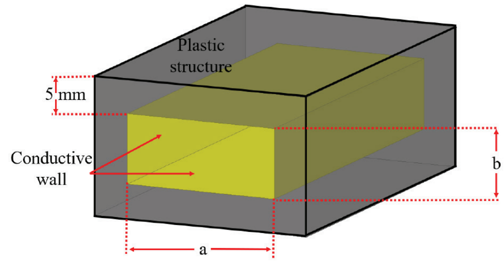

Figure 2. The dimension of the waveguide.

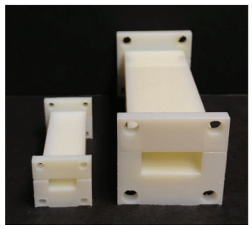

Figure 3. The pre-metallization 3D printed waveguide for K-band and X-band.

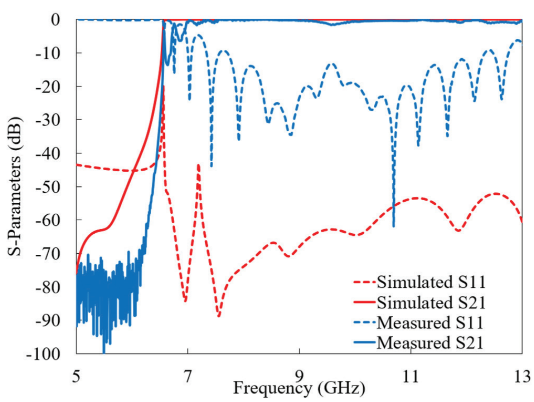

Figure 4. Simulated and measured S-parameters of the X-band waveguide (length = 100 mm).

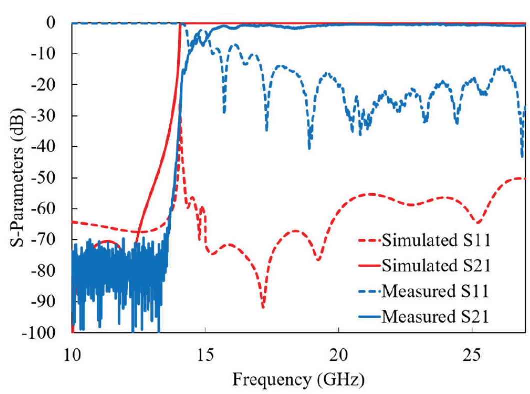

Figure 5. Simulated and measured S-parameters of the K-band waveguide (length = 50 mm).

B. Rectangular Waveguide Iris Filter

Waveguide filters are an essential part of a microwave system such as communication where a selective frequency band can pass (bandpass, low pass or high pass) or blocked (bandstop). One of the popular rectangular waveguide based filter is the iris filter [15]. It consists of

continued on page 14

continued from page 13

multiple metal partitions in the waveguide to form capacitive and inductive regions (high and low impedance regions). Figure 6 shows the schematic of an iris filter along with dimensions used in the design. The 3D printed iris filter before and after metallization is shown in Figure 7 (a) and (b), respectively. Simulated and measured results of the iris filter are shown in Figure 8, and the results match closely. The slight discrepancy of the results is due to the print resolution as well as the surface roughness that cause the extra loss in the measurement. A slight shift in the resonance frequency can be attributed to the fabrication tolerances of slots. In addition, for this structure, there is a slight misalignment between the input port and the waveguide coupler which leads to higher transmission loss, and it can be seen in the measured S_{21} results.

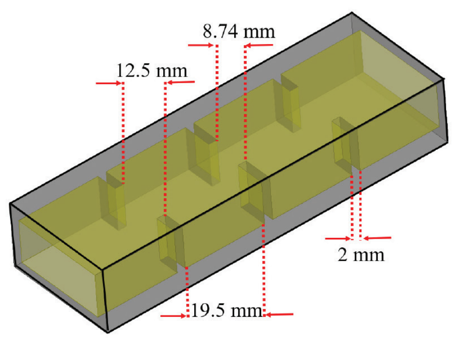

Figure 6. Schematic of a two-pole iris filter.

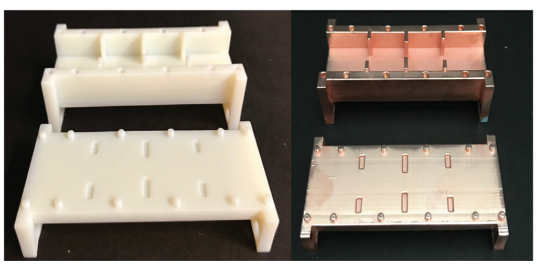

Figure 7. Sections of the fabricated iris filter (a) before and (b) after metal coating.

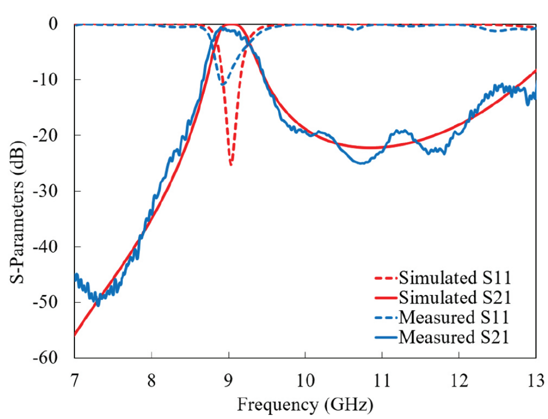

Figure 8. Simulated and measured results of the waveguide iris filter.

C. Leaky Waveguide Antenna

Leaky wave antennas are simple to design and implement as compared to antenna arrays for high gain designs. There are several technologies that can be used to design a leaky wave antenna (e.g., microstrip, substrate integrated waveguides, etc.). Among these, the rectangular waveguide with a slit along the structure, Figure 9, is attractive due to low-loss. In this leaky waveguide design, the slit length and height and depth were designed to achieve high gain at 9 GHz. Figure 10 shows the measured and simulated return loss of the antenna, which shows a wideband operation. The slight discrepancy in these results is due to similar reasons discussed earlier. Figure 11 shows the simulated and measured radiation pattern at 8.8 GHz. The frequency was chosen due to the highest gain measured at this frequency. The measured gain is approximately 10 dBi. The radiation patterns were measured using a Satimo StarLab-18 near-field antenna measurement system. The results show that the simulated and measured results match closely. It also demonstrates that slit dimensions, that are critical in a leaky wave antenna design, be fabricated with high precision using 3D printing. In addition, 3D printing allows for the design of novel slits, not shown here, that can be used to further tailor the radiation pattern and to improve antenna efficiency.

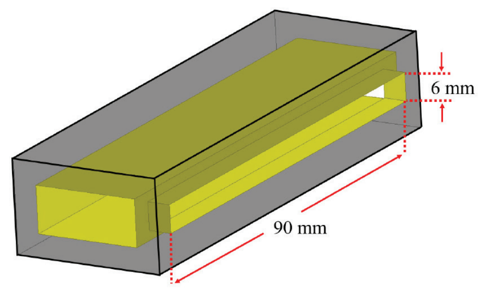

Figure 9. X-band leaky waveguide antenna design.

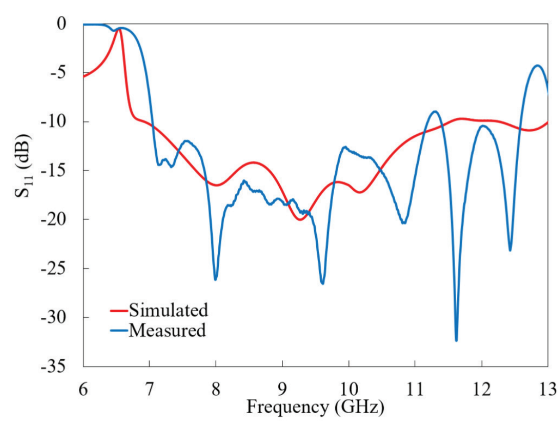

Figure 10. The simulated and measured reflection coefficient of the leaky waveguide antenna.

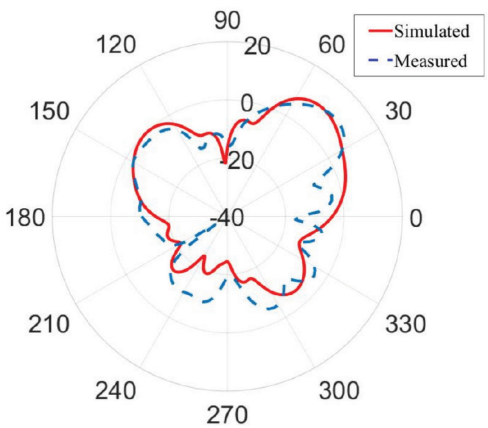

Figure 11. Measured and simulated radiation pattern in the H-plane of the leaky waveguide antenna at 8.8 GHz.

D. Cavity-Backed Slotted Antenna Array

To further demonstrate the possibility of fabricating complex antenna structures through 3D printing, a cavity-backed slotted antenna array was designed and fabricated. Figure 12 shows the cross-sectional view of the 2X4 slotted array based on the design presented in ref. [16]. Figure 13 shows the key printed components before and after assembly. The measured and simulated S_{11} are shown in Figure 14. Figure 15 shows the measured gain as a function of frequency; it shows that high gain over a wide band can be attained using this design. Also shown in the inset of Figure 15 are the simulated and measured radiation patterns at 7.5 and 8.7 GHz, these results match closely. This antenna demonstrates that complex antenna designs can readily be prototyped using 3D printing.

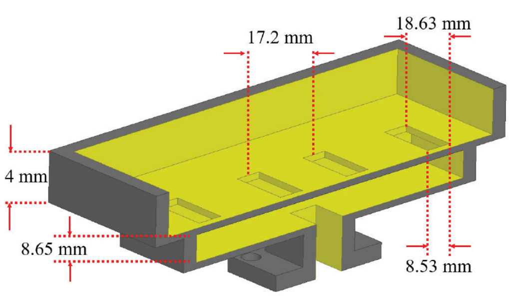

Figure 12. The cross-sectional view of the cavity back slotted antenna array.

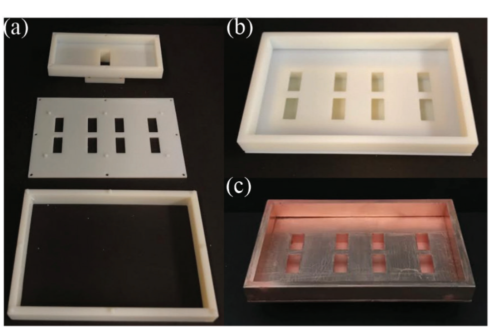

Figure 13. The 3D printed structure of the cavity-backed slotted antenna (a) before and (b) after assembly, and (c) assembled after metal coating.

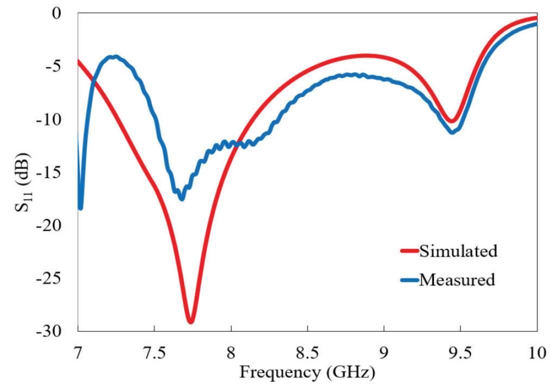

Figure 14. Simulated and measured S_{11} of the cavity-backed slotted antenna array.

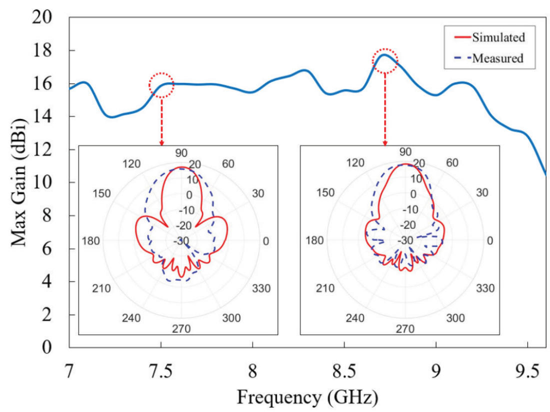

Figure 15. Measured gain of the slotted array. The inset shows the simulated and measured radiation patterns at 7.5 GHz and 8.7 GHz, respectively.

IV. Conclusion

Several 3D printed rectangular waveguide based passive components are demonstrated in this paper. The rectangular waveguides show that low-loss X-band and K-band waveguides are possible. The iris filter demonstrates that 3D printing allows the fabrication of low-loss filters having similar performance to their conventional metallic structures. In addition, a leaky waveguide antenna and a cavity backed slotted array is demonstrated, to the best of our knowledge, for the first time using 3D printing. Antenna arrays demonstrate that complex structures can readily be prototyped using 3D printing. In all the cases, the measured and simulated results matched closely. Overall, this paper demonstrates that high frequency, low-loss, light-weight waveguide-based passive structures can readily be fabricated using 3D plastic printing followed by metal coating. In particular, 3D printing reduces the time between design and prototyping and, a single table-top tool can be used to fabricate complex structures. With further advances in additive manufacturing, RF structures could readily be fabricated directly onto any platform (e.g., the bumper of a car) to make them an integral part of a system, and the design can be changed in real time during manufacturing.

continued on page 16

continued from page 15

Acknowledgment

The authors would like to thank the Electromagnetic Research Group (EMRG) of Michigan State University for helpful discussions, and Mr. Brian Wright from the ECE shop for help with 3D printing.

References

[1] C. Kudsia, R. Cameron and W. Tang. "Innovations in Microwave Filters and Multiplexing Networks for Communications Satellite Systems," *IEEE Transactions on Microwave Theory and Techniques* 40.6, 1992, pp. 1133-1149.

[2] A. R. Barnes, A. Boetti, L. Marchand and J. Hopkins, "An Overview of Microwave Component Requirements for Future Space Applications," *European Gallium Arsenide and Other Semiconductor Application Symposium,* Paris, 2005, pp. 5-12.

[3] D. Pozar, *Microwave Engineering,* 4th ed. Hoboken, NJ: Wiley, 2012.

[4] J. Gundersen and E. Wollack, "Millimeter Wave Corrugated Platelet Feeds," *Journal of Physics:* Conf. Ser. Vol. 155. 2009.

[5] G. Le Sage, "3D Printed Waveguide Slot Array Antennas," *IEEE Access,* vol. 4, pp. 1258-1265, 2016.

[6] M. Ghazali, S. Karuppuswami, A. Kaur and P. Chahal, "3-D Printed Air Substrates for the Design and Fabrication of RF Components," in *IEEE Transactions on Components, Packaging and Manufacturing Technology,* vol.PP, no.99, pp.1-8.

[7] J. Byford, M. Ghazali, S. Karuppuswami, B. Wright and P. Chahal, "Demonstration of RF and Microwave Passive Circuits through 3-D Printing and Selective Metallization," *IEEE Transactions on Components, Packaging and Manufacturing Technology,* vol. 7, no. 3, 2017, pp. 463-471.

[8] A. Kaur, J. Myers, M. Ghazali, J. Byford and P. Chahal, "Affordable Terahertz Components using 3D Printing," *IEEE 65th Electronic Components and Technology Conf.*, San Diego, CA, 2015, pp. 2071-2076.

[9] C. Garcia, R. Rumpf, H. Tsang and J. Barton, "Effects of Extreme Surface Roughness on 3D Printed Horn Antenna," *Electronics Letters*, vol. 49, no. 12, 2013, pp. 734-736.

[10] M. Ghazali, E. Gutierrez, J. Myers, A. Kaur, B. Wright and P. Chahal, "Affordable 3D Printed Microwave Antennas," *IEEE 65th Electronic Components and Technology Conference*, San Diego, CA, 2015, pp. 240-246.

[11] M. Ghazali, K. Park, J. Byford, J. Papapolymerou and P. Chahal, "3D Printed Metalized-polymer UWB High-gain Vivaldi Antennas," IEEE MTT-S *International Microwave Symposium*, San Francisco, CA, 2016, pp. 1-4.

[12] E. Geterud, P. Bergmark and J. Yang, "Lightweight Waveguide and Antenna Components using Plating on Plastics," *2013 7th European Conference on Antennas and Propagation (EuCAP),* Gothenburg, 2013, pp. 1812-1815.

[13] M. D'Auria, W. Otter, J. Hazell, B. Gillatt, C. Long-Collins, N. Ridler and S. Lucyszyn, "3-D Printed Metal-Pipe Rectangular Waveguides," in *IEEE Transactions on Components, Packaging and Manufacturing Technology*, vol. 5, no. 9, 2015, pp. 1339-1349.

[14] K. Park, N. Wiwatcharagoses and P. Chahal, "Wafer-Level Integration of Micro-lens for THz Focal Plane Array Application," *IEEE 63rd Electronic Components and Technology Conference*, Las Vegas, NV, 2013, pp. 1912-1919.

[15] S. Choocadee and S. Akatimagool, "The Simulation, Design and Implementation of Bandpass Filters in Rectangular Waveguides," *Electrical and Electronic Engineering,* 2(3), 2012, pp.152-157.

[16] B. Lee, F. Harackiewicz, B. Jung, and M. J. Park, "Cavity-Backed Slot Antenna Array for the Repeater System of a Satellite Digital Multimedia Broadcasting Service," *IEEE Antennas and Wireless Propagation Letters,* vol. 4, 2005, pp. 389–392.

iMAPS New England 45th Symposium & Expo

May 1, 2018

Boxboro Regency Hotel & Conference Center

Boxborough, Massachusetts

Theme: "*Into the Future Autonomously*"

Keynote Speaker
Chris Jacobs, Vice President, Analog Devices
"Autonomous Transportation & Safety"

Co-Chairs: Lee Levine, PSC & Dave Saums, DS&A

Sessions

**RF & Microwave - Innovations and Emerging Technologies,
Interconnects, Printed Electronics, Novel Packaging Applications,
MEMS, Photonics & Optoelectronics Packaging**

A Few of Our Presentations

5G – The Road Ahead
Thomas Cameron, Analog Devices

Development of Nanomaterial-based Smart Patches and Low-cost MEMS Devices
Cihan Yilmaz, PhD, Flex Boston Innovation Center

The Evolution of a Clinical Grade Wearable Vital Signs Monitor and
the Role of Advanced Microelectronic Packaging Techniques to Increase Functionality
James Ohneck, Exceet

Resonant MEMS Acoustic Switch Package with Integral Tuning Helmholtz Cavity
J. Bernstein, et al., Draper

Printed Electronics Using Magnetohydrodynamic Droplet Jetting of Molten Aluminum and Copper
Denis Cormier, et al., Rochester Institute of Technology

Nanoscale Si3N4 Tuning Fork Cavity Optomechanical Transducers
Rui Zhang, et al., Worcester Polytechnic Institute

For Technical Program Updates, Registration & Information visit www.imapsne.org
Questions on Exhibiting, Sponsoring or Anything Else
Contact Harvey Smith: harveys@imapsne.org or call 508-826-6033

High-Temperature Reliability of Wire Bonds on Thick Film

Zenzhen Shen and Aleksey Reiderman
Baker Hughes, A GE company, 2001 Rankin Road, Houston, TX, US 77072
Ph: 713-879-2652, Email: Zhenzhen.shen@bhge.com

Abstract

In a harsh environment, wire-bonded interconnects are critical for overall reliability of microelectronic assemblies. Aluminum is the dominating metallization of the die wire bonding pads and aluminum wires are used to achieve a monometallic bonding system on the die side. On the substrate side, a monometallic connection is not readily available and typically involves expensive aluminum thin-film deposition or labor-intensive bonding tabs. Nickel-palladium-gold galvanic or electro-less plating stacks are also used to improve bondability and reliability of non-monometallic Al wire bonds on the substrate side. However, these plating stacks do not perform well after excursions above 330°C that are needed for the attachment of die and passives prior to wire bonding. At these temperatures, both palladium and nickel diffuse through the gold and form surface oxides that degrade wire bondability. In monometallic wire-bonding schemes, in addition to aluminum wires gold wires within same assembly are often also needed, for example, when some die is only available with gold-plated bond pads, or to connect substrates to gold-plated pins of hybrid housings. A universal substrate metallization, compatible with aluminum wire and gold wire, is therefore desirable. Thin-film substrates produced by sequential deposition and etching of gold metal, barrier metals, then aluminum metal is a good working solution, but it can be as much as ten times more expensive than other types of substrates. Printed thick-film metallization, a well-established technology, have been widely used for hybrid substrates. Silver-based thick films are inexpensive and capable of accepting aluminum and gold bonds. However, the silver-aluminum bonds are seldom used because of intermetallic formation and subsequent degradation triggered by multiple factors like temperature, humidity, and the presence of halogens. Pd and Pt are often added to the Ag thick films to decrease this effect, but potential usability and the reliability of these formulations in extreme temperature environments is not well researched.

For this study, samples of Pt/Ag thick-film metallization were printed on Al2O3 substrates, and 25-um and 250-um aluminum wires and 50-um gold wires were wedge bonded in daisy chain to the substrate. The test vehicles were subjected to high-temperature testing at 260°C and 280°C. Thermal cycling tests from -20°C to 280°C were also performed. Mechanical and electrical characterizations of the wire bonds were conducted periodically. These tests included resistance and pull-strength measurements. Failure analysis of the bond joints was performed to understand the results of the tests.

The 250-um Al wire and 25-um Al wire showed no significant changes until a critical time-at-temperature was reached. After reaching this temperature, the wire/substrate interface resistance rapidly increased to values as high as 40 Ohms for the 25-um Al wires. However, the pull strength remained within standard throughout the tests of up to 1200 hours. The relationship between time to failure and the temperature is presented in the paper. There was a four times life increase of bonds with every 20°C. With gold wires, no dramatic increase of bond resistance was observed, only a slight increase with time. The pull strength of Au wires remained stable throughout the time at high temperature. The tested Ag/Pt thick film metallization was found to be compatible with bonding of the gold wires and the aluminum wires for high-temperature applications up to an Arrhenius equivalent of 800 hours at 260°C. Additionally, Parylene HT coating was vapor-deposited on one set of 250-um Al wire-bonding samples. This set of samples demonstrated doubling of its useful life as compared to the uncoated samples.

Key words:
wire bonds, MCM, thick film, high-temperature reliability

I. Introduction

There is steady demand for electronics that can be operated in harsh environmental conditions like high temperature, high pressure, vibration and shock. These applications include sensors, well logging and drilling, and control systems for automotive and aerospace. Reliability requirements, miniaturization, and functional sophistication force these applications to be implemented as multi-chip modules and hybrid microelectronic assemblies. Wire-bonded interconnects are critical for overall reliability of microelectronic assemblies. The primary failure mechanism of wire-bonded interconnects is growth of intermetallic compounds at the bond sites. Intermetallic growth is exacerbated by increased operating temperature and by the presence of halogens [1]. Consequently, the material system must be carefully selected. It is well-established that monometallic systems like Au-Au and Al-Al provide the best reliability in high-temperature environments [2]. However, these systems are not always cost effective, particularly in applications where the required life of electronics is relatively short and/or limited by the life of other subsystems.

The predominant wire-bond metallization on the die is aluminum. To obtain a monometallic system at the chip level, aluminum wire is selected. On the substrate side, a monometallic system typically involves expensive aluminum thin-film deposition or labor-intensive bonding tabs. Nickel-palladium-gold galvanic or electro-less plating types are also used to improve bondability and reliability of non-monometallic Al wire bonds on the substrate side. However, these plating types do not perform well after excursions above 330°C that are necessary for attachment of components with high melting point solders like AuSn. At these temperatures, palladium and nickel diffuse through the thin gold and form surface oxides that degrade wire bondability. In addition to aluminum wires, gold wires within the same module are often also required, for example, when some die is only available with gold-plated bond pads, or for bonding to gold-plated package pins. A universal substrate metallization, compatible with aluminum wire and gold wire, is therefore desirable. Thin-film metallized substrates produced by sequential deposition and etching of gold metal, barrier metals, and then aluminum metal is a good working solution, but it is significantly more expensive than other types of substrates. Screen-printed thick-film metallization has been widely used for hybrid substrates for decades [3]. Among various thick-film formulations, silver-based thick films are economical and most universal. They are capable of accommodating aluminum and gold bonding wires, compatible with most adhesives and solders, and provide an exceptional surface for die attachment using sintered silver nano-particle materials [4 - our 1st paper]. However, silver-aluminum wire bonds are rarely used in high-reliability applications because of Ag-Al intermetallic formation and subsequent bond degradation. This degradation is accelerated by factors like high ambient temperature, high relative humidity, and ionic contamination. On the other hand, the degradation is delayed by alloyed additives like Pd and Pt. During the period of initial intermetallic growth, the Ag-Al system remains reliable and is well-suited for short or limited life applications. There is strong correlation between the duration of Ag-Al bond exposure to harsh conditions and the increase in Ag-Al bond's resistance. This correlation allows monitoring of Ag-Al bond quality by monitoring its resistance. If bond resistance exceeds a certain predetermined limit, the device is replaced or settings are adjusted. This approach conforms the well to a condition-based maintenance paradigm.

This study presents the long-term reliability of Al and Au bond wires on Pt/Ag thick-film substrates. The 25-um and 250-um aluminum wires and 50-um gold wires were wedge-bonded in a daisy chain configuration to the test substrates. The test vehicles were subjected to high-temperature aging at 260°C and at 280°C. Thermal cycling tests from -20°C to 280°C were also performed. Mechanical and electrical characterizations of the wire bonds were conducted periodically. These tests included measurements of bond interface resistance and pull strength. Failure analysis of the bond joints was performed to understand the results of the tests. The main objectives of the study were to evaluate electrical and mechanical compatibility of Pt/Ag thick film with Al and Au bond wires, as well as to assess the ability to predict and monitor the degradation of the Ag-Al bonds. The role of Parylene coating in improving reliability of Ag-Al bonds was also evaluated.

II. Test Setup

A. Test setup

Five different thick films were evaluated, and one of the PtAg thick film was selected as the test substrates metallization for its low sheet electrical resistance and good wire bond ability. Test vehicles were screen printed on Al_2O_3 substrate, dried at 150°C and fired at 850°C. The thick-film pattern was designed for mechanical pull test and electrical resistance evaluation, shown in Figure 1. The 25-um and 50-um gold wires were wedge-bonded in a daisy chain to the substrate for electrical testing, and a set of samples were made for mechanical tests. The test vehicles were grouped into two groups. Group A was subjected to high-temperature testing at 260°C while group B was aged at 280°C. Thermal cycling tests from -20°C to 280°C were also performed. Mechanical and electrical characterizations of the wire bonds were conducted periodically. These tests included resistance and pull-strength measurements. Failure analysis of the bond joints was performed to understand the results of the tests.

In addition, the 250-um heavy gauge aluminum wires were bonded on the substrate, with one set of samples coated with Parylene HT, one set of samples without any coating. Both samples were subjected to 280°C aging test for resistant measurement.

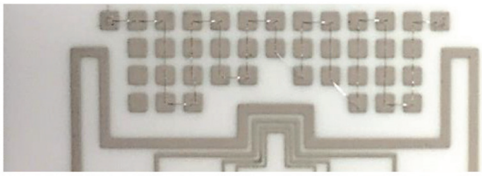

Figure 1. Thick-film test vehicles.

B. Results

Pull test

For the 25-um Al wire, the as-built average pull strength was 4.04cN, with the failure mode of bond lift up. The pull strength recorded for group A aged at 280°C exhibited a slight increase with the aging time. The failure mode remains bond lift up from as built to 200 hours. After 300 hours and 20 thermal cycles, the average pull strength was 4.77cN. The wire broke at the middle of the loop. Group B of 25-um Al wires on thick film were aged

continued on page 20

continued from page 19

in a 260°C oven. The average pull strength displayed similar steady growth with increased time. After 1200 hours, the pull strength was 4.35cN. The failure mode switched from bond lift up to break in the wire after 400 hours of aging. The pull strength results of the 25-um alumina wires on PtAg thick film were summarized in Figure 2, and all the increase percentage was calculated to the initial value.

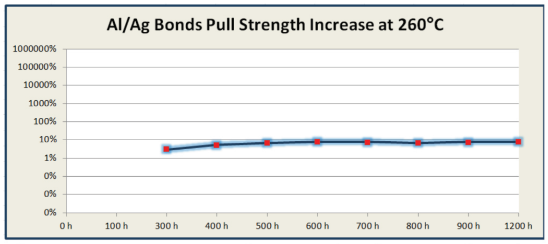

Figure 2. Pull strength of 25-um Al wire on PtAg thick film (260°C aging).

For the 250-um alumina wire on PdAg thick film, the Paralyne HT-coated and uncoated samples were subjected to 280°C aging. The pull strength remained high throughout the test. By the end of the 1200 hours aging at 280°C, the pull strength of both groups exceeded 400cN, and the wire broke in the middle of the loop.

For the 50-um gold wires on PtAg thick film, the as-built samples had an average pull strength of 17.21 cN. During the high-temperature storage at 280°C, the pull strength continued to decrease. After 400 hours of aging, the average pull strength was 9.87cN. The wire break location was at the first bond heel. This failure mode remained the same throughout the test. The test data are shown in Table 1.

Aging at 280°C (Hours)	Pull strength (cN)	Failure mode
0	17.21	1st bond heel
100	13.62	1st bond heel
200	14.8	1st bond heel
300	10.43	1st bond heel
400	9.87	1st bond heel

Table 1. Pull strength of 50um Au wire on PtAg thick film

Interface resistance measurement

Figure 3 plots the resistance increase in percentage at the 25um Al wire and PtAg thick-film interface. At 260°C storage, the resistance of total 74 wire-to-substrate interfaces was 3.085 Ohm before aging. After the first 100 hours of aging, the resistance increased to 4.159 Ohms, and continued to increase slowly but steadily over time. After 900 hours, the resistance was 7.878 Ohms. A significant jump of resistance was observed after 1200 hours of aging, the total interface resistance was 3.2K Ohms.

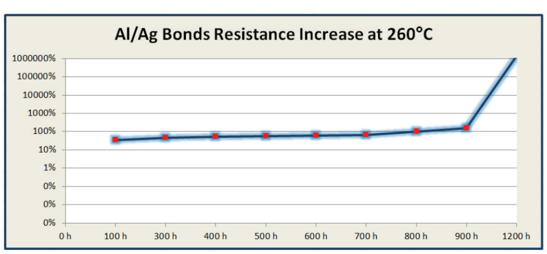

Figure 3. Al/Ag interface resistance change at 260°C.

Another set of 25-um Al wire samples on the PtAg thick film samples were aged at 280°C. The initial resistance of 64 wire-to-substrate interfaces was 2.807 Ohms. The resistance doubled during the first 100 hours of aging, and remained stable throughout 200 hours of testing. A major resistance change was recorded after 300 hours of aging and the total resistance was 1.6K Ohms.

The 50-um Au wires on PtAg thick-film samples were subjected to 280°C high-temperature storage. The initial resistance was 933.7 Ohms, after 400 hours, the total resistance was 1036 Ohms. There was insignificant resistance change throughout the test. Table 2 summarizes the resistance change for the Al and Au wires.

Time at 280°C (Hours)	Resistance of 25-um Al wire (Ohm)	Resistance of 50-um Au wire (mOhm)
0	2.8	933.7
100	4.4	953.2
200	4.9	956.1
300	1600	1006
400	-	1036

Table 2. Resistance change of Al and Au wire on PtAg thick film under 280°C aging

For the 250-um alumina wire on the PdAg thick film, both Parylene HT-coated samples and uncoated samples were subjected to 280°C aging. Before aging, the resistance at the interface of the joint was < 17milliohoms, by the end of the 1200 hours aging at 280°C, the interface resistance of the uncoated sample was 74 ohms, while that of the coated sample was 35 Ohms.

C. Discussion

The thick-film PtAg showed good high-temperature reliability performance with gold wire. Wire pull strength exceeded 8cN after 400 hours of aging at 280°C. The interface resistance between the thick-film PtAg and the gold wire remained stable over the range of temperature being investigated. The resistance is increased by 2% every 100 hours at 280°C.

The 25-um AlSi1% wire on PtAg shows high dependency on environmental exposure. When aged at 260°C, the major resistance increase happened after 1200 hours of aging, while the major increase was observed after 400 hours of aging at 280°C. One thousand hours was defined as the service limit for that type of wire at 260°C. The pull strength remained relatively stable, with a marginal increase throughout the test. The resistance of the bonds, as shown in Figure 3, took approximately 900 hours to double, another 100 hours to triple, and then rapidly stepped up to failure. A similar test conducted at 280°C showed an Arrhenius relationship, with the bond resistance stepping up to failure after approximately 250 hours. This qualification relates to non-hermetic application only. The aluminum/silver bond was a very complex system. Within the first hours, there was rapid growth of aluminum/silver intermetallic compound and formation of a small number of micro cracks. However, this, in itself, was not an immediate failure mechanism. It was the chloride ions that readily penetrated and broke down the aluminum oxide film protecting Al IMCs. At high-temperature operations, the concentration of chloride (Cl-) inside hermetic packages, even with low ionic content epoxy attach materials, will rapidly exceed levels that are typical for non-hermetic packages. Chloride, combined with a few PPMs of available moisture, initiated pitting corrosion, growth of voids, and the subsequent bond's mechanical failure. The absence of this continuous supply of ionics at bond sites in a non-hermetic environment explains why Al/Ag wire bonding works well in such applications but fail inside hermetic enclosures.

For the 250-um diameter Al wire on thick-film PtAg metallization, a major resistance increase was observed at the interface of the wire bonding joint. The sample aged at 280°C for 1000 hours demonstrated a significant resistance increase compared to the initial sample. The cross section showed there was a thin layer of Al_2O_3 formed between the thick film and alumina wire. The data suggests the following two reactions were taking place during high-temperature exposure [5]:

$$Al + Ag \rightarrow AlAg_3 \text{ or } AlAg_2 \quad (1)$$

$$AlAg_3 \text{ or } AlAg_2 + Cl + H_2O \rightarrow Al_2O_3 + Ag + HCL \quad (2)$$

Formula (1) is the formation of the Ag-Al intermetallic, and formula (2) is the decomposition of Ag-Al IMC. The two reactions continue to cycle as long as there is a supply of moisture, ionics, and high temperature. The accumulation of Al and corrosive species result in a continual degradation of the bond joint.

III. Conclusion

Aluminum wire-bonds to PtAg thick-film metallized Al_2O_3 substrate are suitable for 260°C applications up to 1000 hours. The 250-um Al wire and the 25-um Al wire showed no significant changes until a critical time-at-temperature was reached. After reaching this point, the wire/substrate interface resistance rapidly increased to values as high as 40 Ohms for the 25-um Al wires. However, the pull strength remained within standard throughout the tests of up to 1200 hours. The relationship between time to failure and the temperature is presented in the paper. There is a four times life increase of the bonds with every 20°C. No dramatic increase of bond resistance was observed with the gold wires; only a slight increase with time. The pull strength of the Au wires remained stable throughout the time at high temperature. The tested Ag/Pt thick-film metallization was found to be compatible with bonding of the gold and the aluminum wires for high-temperature applications, up to an Arrhenius equivalent of 800 hours at 260°C. Additionally, a Parylene HT coating was vapor-deposited on one set of 250-um Al wire bonding samples. This set of samples demonstrated doubling of its useful life as compared to the uncoated samples.

Control of ionic contamination and moisture is critical for improving wire bonds reliability in high-temperature applications, as those factors will degrade the bond quality. In addition, by adding platinum or palladium in silver-based thick film will improve the reliability of the Ag-Al wire-bonding system.

Additional testing of glob top over wire bonds and failure analysis at different aging stages will be carried on to further evaluate the Al-Ag wire-bonding system for applications requiring short-term exposure to harsh environments.

Acknowledgment

The authors would like to thank Heraeus for its contribution and support in this study.

References

[1] R. Johannessen, F. Oldervoll, F. Strisland, *High temperature reliability of aluminum wire-bonds to thin film, thick film and low temperature co-fired ceramic (LTCC) substrate metallization,* Microelectronics reliability 48 (2008) pp1711-1719.

[2] George G. Harman, *Wire Bonding in Microelectronics*. McGraw Hill, third edition, 2010, pp 164-165.

[3] C. Harper, *Handbook of thick film hybrid microelectronics.* Baltimore, Maryland, 1974, pp. 1-3.

[4] Z. Shen, A. Reiderman, *"Pressure-less AgNP Sintering for High-power MCM Assembly for Extreme Environment Applications,"* IMAPS 2015 annual conference, Oct.27-29 2015, Orlando.

[5] You Cheol Jang, et al. *"Study of Intermetallic Compound Growth and Failure Mechanisms in Long Term Reliability of Silver Bonding Wire,"* 2014 IEEE 16th Electronics Packaging Technology Conference (EPTC), 5 December 2014, Singapore.

IMAPS Raleigh 2017 Award Winners:
BEST of SYMPOSIUM and BEST of TRACK

BEST of TRACK and BEST of SYMPOSIUM

CHIP PACKAGE INTERACTION (CPI)
Session WP1

Advanced CMOS Nodes

Electrical Chip-Board Interaction (e-CBI) of Wafer Level Packaging Technology (048)

Wei Zhao, Qualcomm Technologies (Mark Nakamoto, Karthikeyan Dhandapani, Brian Henderson, Ron Lindley, Riko Radojcic, Urmi Ray, Aurel Gunterus, Mark Schwarz, Ahmer Syed, Vidhya Ramachandran)

BEST of TRACK

HIGH PERFORMANCE, RELIABILITY and SECURITY
Session THP2

Assuring Device Security - Network and Microelectronic Solutions

Nondestructive Imaging of Packaged Microelectronics using Pulsed Terahertz Technology (160)

Magda El-Shenawee, University of Arkansas (Tyler Bowman)

ADVANCED PACKAGING and ENABLING TECHNOLOGIES
Session THA3

Fanout Wafer Level Packaging

Implementation of Wafer Level Packaging KOZ using SU-8 as Dielectric for the Merging of WL Fan Out to Microfluidic and Bio-Medical Applications (118)

Steffen Kroehnert, Amkor Technology (formerly Nanium) (Andre Cardoso, Raquel Pinto, Elisabete Fernandes)

ADVANCED PACKAGING and SYSTEM INTEGRATION
Session WP4

Wire Bonding

Wire Bonding Looping Solutions for High Density System-in-Package (SiP) (151)

Basil Milton, Kulicke & Soffa (Odal Kwon, Cuong Huynh, Ivy Qin, Bob Chylak)

ADVANCED MATERIALS and PROCESSES
Session TP5

Novel Materials/Processes I

Alternative Deposition Solution for Cost Reduction of TSV Integration (034)

Julien Vitiello, KOBUS (Fabien Piallat)

Student Awards
IMAPS Raleigh 2017

Best Student Paper of Symposium Award

WA36

Inkjet and 3D Printing Technology for Fundamental Millimeter-Wave Wireless Packaging

Bijan Tehrani
Georgia Institute of Technology
btehrani3@gatech.edu

Outstanding Student Paper Awards

WA45

Atmospheric Probe for Real Time Weather Monitoring

J. Craig Prather
Auburn University
jcp0022@auburn.edu

THA25

Thermal and Viscoelastic Properties of Underfills Using Hexagonal Boron Nitride (hBN) Nanofiller

Sara Abbasirazgaleh
North Carolina A&T State University
s.a.razgaleh@gmail.com

THA46

Multi-Factor Product Authentication Using Integrated Quick Response (QR) Code Antenna

John Doroshewitz
Michigan State University
doroshe2@msu.edu

Best Student Poster Award

Rapid Prototyping Tape Stencils for the Application of Solder Paste

Mimi Yang
Stanford University
mxy@stanford.edu

Announcement and Call for Abstracts

International Conference and Exhibition on

High Temperature Electronics (HiTEC)

www.imaps.org/hitec

May 8-10, 2018
Hotel Albuquerque
Albuquerque, New Mexico USA

Overview: HiTEC 2018 continues the tradition of providing the leading biennial conference dedicated to the advancement and dissemination of knowledge of the high temperature electronics industry. Under the organizational sponsorship of the International Microelectronics Assembly and Packaging Society, HiTEC 2018 will be the forum for presenting leading high temperature electronics research results and application requirements. It will also be an opportunity to network with colleagues from around the world working to advance high temperature electronics.

Abstracts being requested include the following topics:

- **Applications:**
  - Geothermal
  - Oil well logging
  - Automotive
  - Military/aerospace
  - Space
- **Device Technologies:**
  - Si, SOI
  - SiC
  - Diamond
  - GaN
  - GaAs
  - Contacts
  - Dielectrics
- **MEMS and Sensors:**
  - Vibration
  - Pressure
  - Seismic
- **Packaging:**
  - Materials
  - Processing
  - Solders/Brazes
  - PC Boards
  - Wire Bonding
  - Flip Chip
  - Insulation
  - Thermal management
- **Circuits:**
  - Analog
  - Digital
  - Power
  - Wireless
  - Optical
- **Energy Sources:**
  - Batteries
  - Nuclear
  - Fuel Cells
- **Passives:**
  - Resistors
  - Inductors
  - Capacitors
  - Oscillators
  - Connectors
- **Reliability:**
  - Failure mechanisms
  - Experimental and modeling results

Student Competition sponsored by the Microelectronics Foundation:

The Microelectronics Foundation sponsors ***Student Paper Competitions*** in conjunction with all Advanced Technology Workshops (ATWs) and Conferences. Students submitting their work and identifying that "Yes, I'm a full-time student" on the abstract submission form, will automatically be considered for these competitions. The review committee will evaluate all student papers/posters and award a total of $1,000 in award checks at the ATW/Conference. The selected student(s) must attend the event to present his or her work and receive the award. For more information on the student competition, go to www.microelectronicsfoundation.org.

Your IMAPS Member Benefits at Your Chapter Level

Your participation in these IMAPS chapter events greatly increases the value of your member benefits by providing industry insight, technical information, and networking opportunities. See more event information at www.imaps.org/calendar

Central Texas

The Central Texas (Austin) chapter of IMAPS had an interesting meeting February 13, 2018 with presentations by Ian Wong from National Instruments (Role of 5G and Low-Power Wireless in Connected World), Todd Humphreys from UT-Austin (Trusted Automated Vehicles), Colin Tompkins from Silicon Labs (Next Generation Biometric Sensors in Wearables), and Donnie Garcia from NXP (Designing Secure IoT Devices Starts with a Secure Boot). We had a good turnout and everyone seemed to enjoy the cookies, pizza, and conversation.

The next meeting is being planned for May 15, 2018.

Ian Wong, National Instruments, presents "Role of 5G and Low-Power Wireless in Connected World."

Chapter members and guests all enjoying conversation and pizza.

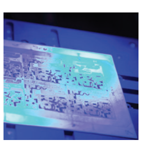

IMAPS/ACerS 14th International Conference and Exhibition on

Ceramic Interconnect and Ceramic Microsystems Technologies (CICMT 2018)

18-20 April 2018
University of Aveiro
Aveiro, PORTUGAL

General Chair:
Paula Vilarinho
University of Aveiro
paula.vilarinho@ua.pt

General Co-Chair:
Robert Pullar
University of Aveiro
rpullar@ua.pt

Technical Chair:
Steve Dai
Sandia National Labs.
sxdai@sandia.gov

Technical Co-Chair:
Yongxiang Li
Shanghai Institute of Ceramics
yxli@mail.sic.ac.cn

Goal
The Ceramic Interconnect and Ceramic Microsystems Technologies (CICMT) conference brings together a diverse set of disciplines to share experiences and promote opportunities to accelerate research, development and the application of ceramic interconnect and ceramic microsystems technologies. This international conference features ceramic technology for both microsystems and interconnect applications in a dual-track technical program. The Ceramic Interconnect track focuses on cost effective and reliable high performance ceramic interconnect products for hostile thermal and chemical environments in the automotive, aerospace, lighting, solar, defense/security, and communications industries. The Ceramic Microsystems track focuses on emerging applications and new products that exploit the ability of 3-D ceramic structures to integrate interconnect/packaging with microfluidic, optical, micro-reactor and sensing functions. Tape casting, thick film hybrid, direct write and rapid prototyping technologies are common to both tracks, with emphasis on materials, processes, prototype development, advanced design and application opportunities.

Ceramic Interconnect Track
Conventional thick and thin film ceramic technologies are being revolutionized and extended through the development of low temperature co-fired ceramics, photo patterning, and embedded passive component materials and processes. These have contributed to increased circuit density, enhanced functionality, and improved performance that are being adopted for leading edge applications in wireless and optical communications, automotive, MEMS, sensors, and energy. Data communications and the Internet are driving the demand for bandwidth, sparking demand for optical communication equipment and new interconnect and packaging applications that perform at 40 Gb/sec and beyond. In under-the-hood electronics for automotive, engine/transmission control, communications, and safety applications continue to drive the growth of ceramic interconnect technology, while collision avoidance systems are creating interest in low loss ceramic materials for frequencies approaching 100 GHz.

Ceramic Microsystems Track
Enabled by the availability of commercial ceramic, metal and embedded passives materials systems, and the rapid prototyping capabilities of the well established multilayer ceramic interconnect technology, three dimensional (3-D) functional ceramic structures are spawning new microsystems applications in MEMS, sensors, microfluidics, bio-devices, microreactors, and metamaterials. These new devices and applications exploit the ability to integrate complex 3D features and active components (e.g., valves, pumps, switches, light pipes, and reaction chambers).

In addition, the Ceramic Microsystems track of the CICMT conference targets new developments in microsystems that include fabricating 3-D micro device structures enhanced with sol-gel, advanced printing and patterning technologies, high temperature materials technologies, and emerging applications like energy harvesting. Many of these innovative applications are taking advantage of the unique ability to integrate the thermal, chemical, mechanical and electrical properties of these multicomponent ceramic-metal systems.

Special Features
- Invited keynote and international presentations on the current status ceramic technology and future system directions.
- A focused exhibition for suppliers who support the use of the technologies.
- A technical poster session to promote student participation.
- Social events to promote new contacts.

IMAPS/ACerS 14th International Conference and Exhibition on

Ceramic Interconnect and Ceramic Microsystems Technologies (CICMT 2018)

Planned Session and Paper Topics Include:

Ceramic Microsystems

Markets and Applications
- MEMS Technology and Markets
- Batteries and Fuel Cells
- Biological and Medical
- Chemical and Biochemical
- Photonics

Materials and Properties
- Materials Integration and Nano-materials
- Thermal Management and Reliability
- Piezoelectric Materials
- Optoelectronics

Processing and Manufacturing
- MEMS Manufacturing Technology
- Industrial Automation and Rapid Prototyping
- Nano-technology/Integration
- High Temperature Microsystems

Devices
- Sensors and Actuators
- Micro-reactors
- Fluidic Devices
- Biomolecular and Cell Transport Systems
- Energy Conversion Systems

Characterization and Reliability
- Materials and Process Characterization
- Systems Reliability, Lifetime, and Failure Estimation
- Reliability of High-Performance Microsystems

Design, Modeling, and Simulation
- Thermal and Heat Transfer
- Computational Fluid Dynamics

Ceramic Interconnect

Markets and Applications
- Automotive
- Aerospace
- Lighting/Solar
- Wireless/Communication
- Medical Electronics

Materials and Properties/Functions
- Dielectric and Magnetic Materials
- Embedded and Integrated Passives
- Microwave/mm Wave Characterization
- Zero-shrink Ceramic Systems

Processing and Manufacturing
- LTCC and Multilayer Ceramics
- Roll to Roll and Continuous Manufacturing
- Direct WRite and Drop on Demand
- Advanced Thick Film Processing
- Fine Structuring Technologies

Devices
- Circuits, Antennas, and Filters
- Embedded Structures and Components
- Optical Devices and Optoelectronics

Characterization and Reliability
- Characterization of Green Tapes
- Life Testing, Quality Issues
- RF Performance

Design, Modeling, and Simulation
- High Frequency Design Software
- Design Rules

Integrated Ceramic Technology

Advanced Packaging Technology
- Next Generation Packaging Technologies
- Packaging and Integration in BioMEMS
- Packaging Issues for MEMS Devices
- Technologies for Microsystems Components and Substrates
- Packaging Standard for Microsystems
- Environmental Issues, Lead Free Systems
- Cost Reduction

For more information visit

www.imaps.org/ceramics

Topical Workshop and Tabletop Exhibition on

WIRE BONDING

www.imaps.org/wirebonding

October 8, 2018
Pasadena Convention Center, Pasadena, CA

General Chair:
Lee Levine | Process Solutions Consulting | Phone: 610-248-2002 | levilr@ptd.net

Wire Bonding Workshop Organizing Committee:
Bob Chylak, K&S; William Crockett, Tanaka; Doug Day, Shinkawa; Dodgie Calpito, SPT; Dan Evans, Palomar; Mark Greenwell, Coorstek; Horst Clauberg, K&S; Ivy Qin, K&S; Leroy Christie, ASM; Amy Low, Heraeus; Mike Mckeown, Hesse Mechatronics; Josef Sedimair, F&K Delvotec; Uri Zaks, MPP Tools; Wenjuan Qi, Palomar; Bob Whitlock, SPT; Winston Bautista, SPT

ABSTRACTS DUE: MARCH 30, 2018

New 1-Day Workshop Format – Maximum of 12 Speaking Spots Available

Wire Bonding Workshop Focus:
The objective of the Wire Bonding Workshop is to have a unique forum that brings together scientists, engineers, manufacturing, academia, and business people from around the world who have been working in the area of Wire Bonding. This workshop has been specifically organized to allow for the presentation and debate of some of the latest and hottest technologies out there related to the use of Wire Bonding in semiconductor and microelectronic packaging.

- Cu/Low-K packaging processes
- Terminal pad structures and modifications
- Cu/Low-K packaging materials
- Assembly processes and handling issues
- Wirebonding and bumping
- Novel packaging and design
- Failure analysis and reliability
- Electromigration and interfacial adhesion
- Testing and probing challenges
- Simulation and modeling

Those wishing to present at the Wire Bonding Topical Workshop must submit a ~300 word abstract electronically **BEFORE MARCH 30, 2018**, using the on-line submittal form at: www.imaps.org/abstracts.htm. Full written papers are not required. All Speakers are required to pay a reduced registration fee and are required to attend the entire workshop to make the presentation in-person. Please contact Brian Schieman by email at bschieman@imaps.org if you have questions or need assistance submitting an abstract.

Co-located with IMAPS 2018

IMAPS 2018 PASADENA
51st International Symposium on Microelectronics
October 8-11, 2018
Pasadena Convention Center

kester®

Kester Launches NF1060-VF Eco-Friendly Soldering Flux

Visit Kester's booth (#3118) at APEX 2018!

ITASCA, IL — February 19, 2018, Kester is proud to announce the launch of NF1060-VF, a new addition to Kester's No-Clean, VOC-Free product line. NF1060-VF is a zero-halogen (none intentionally added) wave soldering flux that maintains its soldering performance achieving excellent through-hole fill and low-defect soldering of lead-free electronic circuit board assemblies. NF1060-VF is ORM0 per J-STD-004B, VOC-Free for lower VOC emissions and has a low solids content which prevents clogging or buildup around flux spray nozzles.

For additional information on this product including technical and safety data sheets, please see https://www.kester.com/products/product/nf1060-vf-soldering-flux.

For any questions or additional information, please contact Fil Marcial-Hatfield, Global Product Manager at fmarcial@kester.com or Michelle O'Brien, Marketing & Communications Specialist.

***

Kester is a global supplier of assembly materials for the Electronic Assembly and Semiconductor Packaging industries. Kester is focused on delivering innovative, robust and high-quality solutions to help our customers address their technological challenges. Kester's current product portfolio includes soldering attachment materials such as solder paste, soldering chemicals, TSF (tacky solder flux) materials, and metal products such as bar, solid and flux-cored wire. Kester is an Illinois Tool Works (ITW) company. ITW is a Fortune 200 company that produces engineered fasteners and components, equipment and consumable systems, and specialty products. It employs approximately 49,000 people, and is based in Glenview, Illinois, with operations in 57 countries.

UPDATES FROM IMAPS

UPDATES FROM IMAPS

Premier Corporate Members

IMAPS has introduced a new level of support for corporate members. These companies have decided to participate in our Society at the Premier Corporate Member level. We are extremely grateful for the dedication to the furtherance of our educational opportunities and technological goals.

Amkor Technology®

MST
Micro Systems Technologies
engineering for life

ASE GROUP

MRSI SYSTEMS™

Canon

NGK SPARK PLUGS | NTK TECHNICAL CERAMICS
NGK SPARK PLUG CO., LTD.

EMD Performance Materials

PALOMAR™ TECHNOLOGIES

Honeywell

PLEXUS®
The Product Realization Company

INDIUM CORPORATION®

Promex
Microelectronics Assembly Technologies

QUALCOMM®

kester®

Quik-Pak™
Microelectronic Packaging & Assembly Solutions

KYOCERA

Raytheon

MASTERBOND®
ADHESIVES | SEALANTS | COATINGS
Helping engineers meet specific requirements

SCS
SPECIALTY COATING SYSTEMS™

Welcome New IMAPS Members!

November-December 2017

Organizational Members
Wacker Chemical Corp.
Sputtering Components, Inc.
Neutronix Quintel

Individual Members
Guy Abarbanel
Ghassan Abu-Hamdeh
Alkim Akyurtlu
James Barry
Stefan Behler
Basar Bolukbas
Pavel Borodulin
Michael Borrelli
Jonathan Cetier
Alex Chan
Vamsy Chodavarapu
Eugene Chow
Wayne Churaman
Robert Crowell
Juan Cruz
Michael Current
Bo Dan
Rebecca Dean
David Deisenroth
Jeffrey Demmin
Sorin Dinescu
Bruce Drolen
Stephan Fatschel
Phil Ferguson
Hector Fonseca
Gilles Fresquet
Gilbert Galindo
Bo Gao
Kanchan Ghosal
Michael Grubisich
Yi Guo
Dinesh Gupta
Deborah Hagen
Richard Hamilton
Steve Hammond
Deny Hanan
Jiangqi He
David Hill
Carl Hinshaw
John Holaday
Michael Holmes
Xiaopeng Huang
Erin Hurbi
Subu Iyer
Richard Joyce
Andrew Kelly
James (Ji Yun) Kim
Markus Kreitzer
Lawrence Kushner
Lee Hyun Kyu
Michael Lee
Young Kyu Lee
Zhihua Li
William Little
Xiao Hu Liu
Richard Mallalieu
Vikram Manthri
Dawn Mantz
Nicholas Mescia
Christopher Michael
Shelby Nelson
Steven Nelson
Jackie Nguyen
Michael Nikkhoo
Pascal Oberndorff
Megan Olson
John Osenbach
Janet Ozasa
Jason Papka
Russ Pina
Yin Qian
Sebastien Quenard
Vicki Ragogna
Tarak Railkar
Suresh Ramalingam
V N N Trilochan Rambhatla
Andras Resch
Bradley Richard
Tyler Richier
Hua Rong
Emily Sataua
Franz Schrank
Shye Shapira
Toshimasa Shimoda
Hossein Shirangi
Rick Stevens
Prashanth Subramanian
Mark Swartz
Eli Symm
Yoshiaki Takemoto
Bijan Tehrani
Christopher Tipp
Albert Torres
Pouria Valley
Markus Valtere
Hayato Wakabayashi
Dongyi Wang
Jeremy Ward
David Whitney
Mark Wold
Elyn Xu
Masahiro Yamamoto
Tak Sang Yeung
Jun Yu
Zhengya Zhang

CHAPTER CONTACTS

CHAPTER NAME	CONTACT	E-MAIL
Angel	Leadership recruitment in progress	Interested? Contact Brianne Lamm blamm@imaps.org
Arizona	Sean Ferrian	sean@ferrian.com
California Orange	Bill Gaines	William.gaines@ngc.com
Chesapeake	Lauren Boteler	Lauren.m.boteler.civ@mail.mil
Carolinas	Leadership recruitment in progress	Interested? Contact Brianne Lamm blamm@imaps.org
Central Texas	Kevin Hess	k.hess@utexas.edu
Cleveland/Pittsburgh	John Mazurowski	jmazurowski@eoc.psu.edu
Empire	Benson Chan	chanb@binghamton.edu
Florida	Mike Newton	Mike@Newtoncyberfacturing.com
Garden State	Leadership recruitment in progress	Interested? Contact Brianne Lamm blamm@imaps.org
Greater Dallas	Sam Forman	sam.forman@m-coat.com
Indiana	Larry Wallman	lwallman@sbcglobal.net
Metro	Scott Baldassarre	Scott.Baldassarre@L-3com.com
New England	Jon Medernach	jon.medernach@mrsisystems.com
NorCal	David Towne	dtowne@comcast.net
Northwest	Leadership recruitment in progress	Interested? Contact Brianne Lamm blamm@imaps.org
San Diego	Iris Labadie	iris.labadie@kyocera.com
Viking	Mark Hoffmeyer	hoffmeyr@us.ibm.com
Germany	Ernst Eggelaar	ee@microelectronic.de
France	Florence Vireton	Imaps.france@imapsfrance.org
United Kingdom	Andy Longford	Andy.longford@imaps.org.uk
Taiwan	Wun-Yan Chen	wunyan@itri.org.tw
Nordic	Terho Kutilainen	treasurer@imapsnordic.org
Benelux	Katrien Vanneste	Katrien.vanneste@elis.ugent.be
Italy	Marta Daffara	info@imaps-italy.it
Japan	Orii Yasumitsu	ORII@jp.ibm.com

ADVERTISER HOTLINE

ADVERTISER	CONTACT	TELEPHONE	EMAIL	WEBSITE	PAGE
IMAPSource	Brian Schieman	412-368-1621	bschieman@imaps.org	www. imaps.org	31
Indium	Rick Short	315-381-7554	rshort@indium.com	www.indium.com	11
Master Bond	Robert Michaels	201-343-8983	info@masterbond.com	www.masterbond.com	5, 29
Mini-Systems, Inc.	Craig Tourgee	508-695-0203	ctourgee@mini-systemsinc.com	www.mini-systemsinc.com	back cover

Advancing Microelectronics
2018 Editorial Schedule

Issue	Theme	Copy Deadline	Ad Commitment I/Os Deadline
May/Jun	Heterogeneous Integration – System in Package (SiP)	Mar. 8	Mar. 13
Jul/Aug	IMAPS 2018 (Pasadena) Show Issue	May 8	May 14
Sep/Oct	Advanced Materials and Additive Manufacturing	Jul. 6	July 13
Nov/Dec	Chip Package Integration (CPI)	Sep. 7	Sep. 13

IMAPS HEADQUARTERS

WHO TO CALL

Michael O'Donoghue, Executive Director, (919) 293-5300, modonoghue@imaps.org, Strategic Planning, Contracts and Negotiations, Legal Issues, Policy Development, Intersociety Liaisons, Customer Satisfaction

Brian Schieman, Director of Programs, (412) 368-1621, bschieman@imaps.org, Development of Society Programs, Website Development, Information Technology, Exhibits, Publications, Sponsorship, Volunteers/Committees

Ann Bell, Managing Editor, *Advancing Microelectronics,* (703) 860-5770, abell@imaps.org, Coordination, Editing, and Placement Management of all pieces of bi-monthly publication, Advertising and Public Relations

Brianne Lamm, Marketing and Events Manager, (980) 299-9873, blamm@imaps.org, Corporate Membership, Membership and Event Marketing, Society Newsletters/Emails, Event Management, Meeting Logistics and Arrangements, Hotel and Vendor Management

Shelby Moirano, Membership Administration, (919) 293-5000, smoirano@imaps.org, Member Relations and Services, Administration, Dues Processing, Membership Invoicing, Foundation Contributions, Data Entry, Mail Processing, Address Changes, Telephone Support

CALENDAR OF EVENTS

2018	start	end	
APRIL	4-18-18	4-20-18	CICMT 2018 (PORTUGAL) University of Aveiro Aveiro, Portugal www.imaps.org/ceramics
MAY	5-1-18	5-1-18	IMAPS New England - 45th Symposium & Expo Boxborough, MA www.imapsne.org
	5-8-18	5-10-18	HiTEC 2018 - High Temperature Electronics Albuquerque, New Mexico www.imaps.org/hitec
OCTOBER	10-8-18	10-8-18	Topical Workshop & Tabletop Exhibition on Wire Bonding Pasadena, CA www.imaps.org/wirebonding
	10-8-18	10-11-18	IMAPS 2018 - Pasadena Pasadena, CA www.imaps.org/imaps2018

Visit www.imaps.org

for links to all upcoming events including:

- full event descriptions
- abstract submissions
- exhibition information
- event updates